

LiDAR-Based Place Recognition For Autonomous Driving: A Survey

Pengcheng Shi, Yongjun Zhang, Jiayuan Li

Abstract—LiDAR-based place recognition (LPR) plays a pivotal role in autonomous driving, which assists Simultaneous Localization and Mapping (SLAM) systems in reducing accumulated errors and achieving reliable localization. However, existing reviews predominantly concentrate on visual place recognition (VPR) methods. Despite notable advancements in LPR in recent years, there is yet a systematic review dedicated to this field to the best of our knowledge. This paper bridges the gap by providing a comprehensive review of place recognition methods employing LiDAR sensors, thus facilitating and encouraging further research. We commence by delving into the problem formulation of place recognition and exploring existing challenges, describing relations to previous surveys. Subsequently, we conduct an in-depth review of related research, which offers detailed classifications, strengths and weaknesses, and architectures. Finally, we summarize existing datasets, commonly used evaluation metrics, and comprehensive evaluation results from various methods on public datasets. This paper can serve as a valuable tutorial for newcomers entering the realm of place recognition and researchers interested in long-term robot localization. We pledge to maintain an up-to-date project on our website <https://github.com/ShiPC-AI/LPR-Survey>.

Index Terms—SLAM, LiDAR-based Place Recognition, Loop Closure Detection, Map Localization.

1 INTRODUCTION

PLACE recognition [1], [2], [3], [4], [5], [6], [7], [8] is a challenging and ongoing research problem that aims to identify previously visited places across different viewpoints and environments. This task holds great significance in various robotic applications. Firstly, long-term localization [9], [10], [11] and place retrieval [12], [13], [14] address the issue of localization in changing environments. Secondly, place recognition [15], [16], [17], [18] facilitates real-time loop closure detection (LCD) to create drift-free global maps. Thirdly, metric localization [19], [20], [21] within prior maps offers a reliable means to recover the kidnapped vehicle's poses.

Sensor observation-based methods [22], [23], [24], [25], [26], [27] outperform traditional global positioning system (GPS) [28], [29], inertia measurement unit (IMU) [30], [31], [32], and wheel odometers [33] in autonomy, flexibility, anti-interference capability, independence from geomagnetic signals, and cost-effectiveness. Despite significant research advancements and the emergence of numerous methods in recent years, place recognition remains challenging due to viewpoint differences, occlusions, data variations, long-term changes, and computational complexity. To facilitate and encourage further research, scholars have engaged in method classification [34], performance evaluation [35], [36], challenge summarization [37], and prospect prediction [38] based on the current progress in this field. However, existing work primarily focuses on VPR, necessitating a comprehensive and systematic review of LPR to bridge this gap.

This work was supported by the National Natural Science Foundation of China (NSFC) under Grant 42030102 and 42271444, and the Science and Technology Major Project of Hubei Province under Grant 2021AAA010.

Pengcheng Shi is with the School of Computer Science, Wuhan University, Wuhan 430072, China

Yongjun Zhang and Jiayuan Li are with the School of Remote Sensing and Information Engineering, Wuhan University, Wuhan 430079, China (Corresponding authors: Yongjun Zhang, Jiayuan Li)

In this paper, we presents a comprehensive review of LPR research, accompanied by a detailed methodological taxonomy depicted in Figure 1. We categorize each method into handcrafted and learning-based approaches and then subdivide them into more types, providing detailed introductions to pioneering works. This well-organized layout enhances reading efficiency and facilitates a better understanding of the relevant technologies in place recognition. Our main contributions are as follows:

- To the best of our knowledge, this paper is the first survey exclusively focusing on place recognition based on 3D LiDAR. We delve into the problem formulation, challenges, and the relationship to previous surveys.
- We provide an in-depth overview of LPR covering conventional handcrafted descriptors and advanced deep-learning techniques. We classify existing methods into seven categories and describe their advantages and limitations.
- We incorporate numerous figures and tables to help readers understand the open-source code, backbone networks, feature types, similarity metrics, memory costs, training strategies, running efficiency, and localization capabilities of these methods.
- We summarize existing datasets and evaluation metrics while comprehensively comparing existing methods on several public datasets. In addition, we also provide a regularly updated project.

The structure of this paper is as follows. Section 1 summarizes our contributions and paper structures. Section 2 describes the research background. From Section 3 to 9, we comprehensively review recent methods and offer detailed classifications. Section 10 collects existing datasets, evaluation metrics, and performance comparisons on pub-

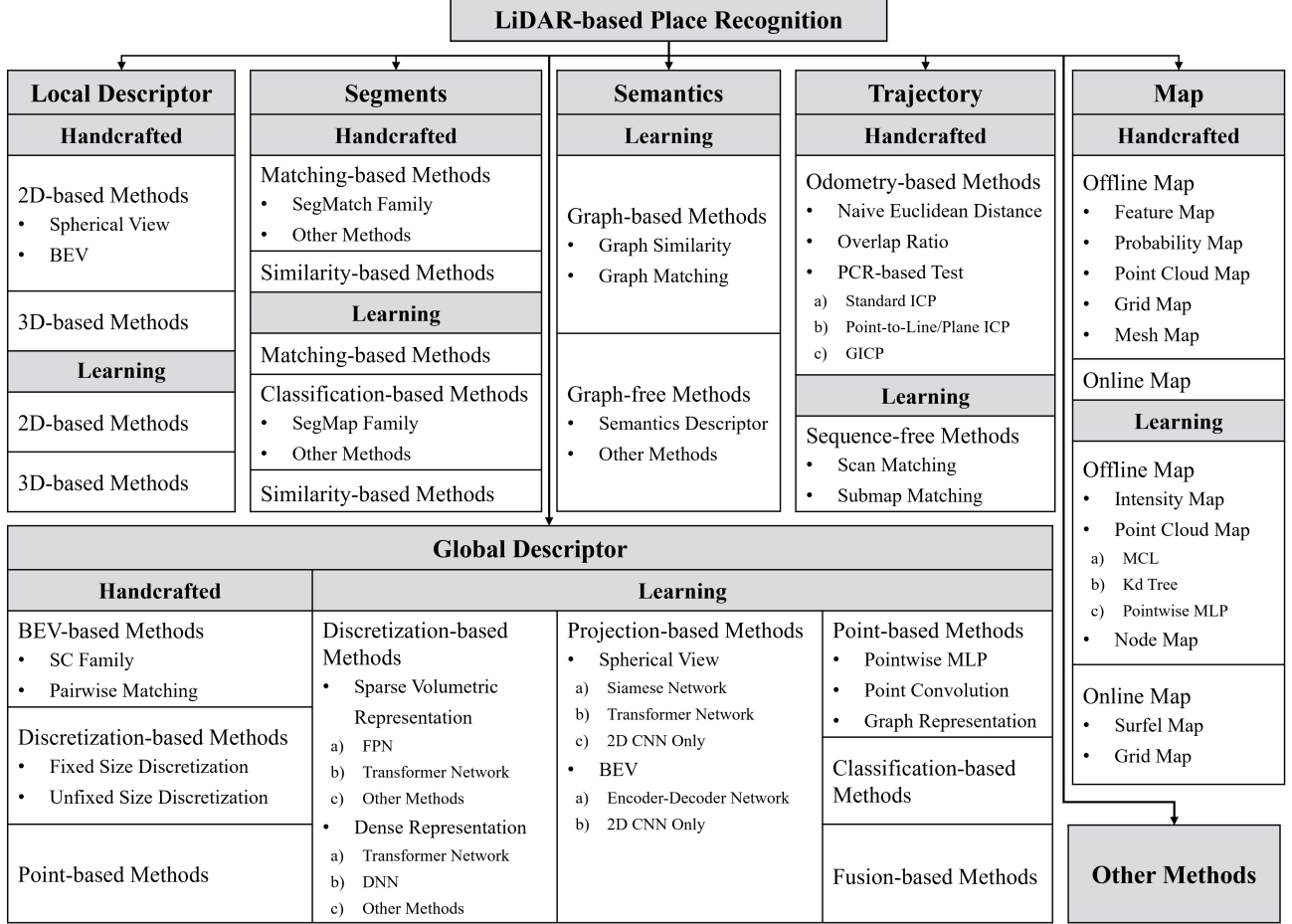


Figure 1: A taxonomy of LPR methods.

lic datasets. Finally, Section 11 concludes the paper and presents promising future directions.

2 BACKGROUND

2.1 Problem Formulation

The place recognition task is commonly categorized into three main groups: place retrieval, LCD, and map localization. Given a query data X and reference database D , place retrieval and LCD can be formulated as:

$$\hat{Y} = \arg \max_Y p(X, Y | Y \in D) \quad (1)$$

where Y represents a matching candidate for X and \hat{Y} is the best-matched one. $p(X, Y | Y \in D)$ is a similarity or matching score. Place retrieval commonly creates offline databases from pre-collected or generated sequences, while LCD uses real-time SLAM data for constructing databases.

Map localization involves utilizing a high-definition map (HD Map) and data association techniques to compute the global pose, formulated as:

$$\hat{Y}, \mathbf{T} = \arg \max_Y p(X, Y | Y \in D) \quad (2)$$

where \mathbf{T} is a transformation with six or three degree-of-freedoms (DoF). The database D typically comprises prior map and reference data. This method allows for direct pose comparison, making it applicable in single and multiple robot systems.

2.2 Challenges of LPR

With the advancements in image processing technologies [39] and the availability of affordable equipment, numerous vision-based methods [1], [40], [41], [42] have emerged over the past decades. However, these methods encounter challenges such as illumination variations, viewpoint changes, adverse weather conditions, and scale ambiguity. In contrast, LiDAR sensors actively emit laser signals to capture high-resolution 3D points, which excel in providing precise and detailed geometric information [43] even in low-light conditions. In addition, the rapid progress of 3D scanning technology further fuels the interest in place recognition research using LiDAR sensors.

Numerous recent LPR methods have explored techniques like bird-eye-view (BEV) [4], [44], [45], histograms [46], [47], image representations [9], [48], and graph theory [49], [50], [51] to enhance performance. They achieve rotational invariance through brute-force search [4], [44] and frequency domain analysis [45], [52]. Additional approaches employ pose proximity [53], [54], sequence matching [6], [55], and point cloud registration (PCR) [56], [57], [58] techniques to improve recognition accuracy. However, these methods struggle in dynamic and highly occluded environments. Traditional methods rely on low-level features (coordinates [59], normals [60], intensities [61], [62], [63], range [64] and density [65]), while learning-based approaches gradually show promising results using neural networks

[66], [67], attention mechanisms [68], [69], semantics [70], [71], and classifiers [72]. Furthermore, diverse map representations, such as point clouds [73], semantics [74], and mesh [75], have been successfully applied in map localization. Despite the impressive results claimed by these methods, several challenges persist that require further attention:

- **Motion Distortions:** The common assumption of constant velocity motion [76], [77] is inaccurate for deskewing distorted scans, especially in high-speed applications.
- **Viewpoint Differences:** Lane-level horizontal deviations may exist when a robot revisits a historical place from different directions. While a few methods [4], [9], [44], [49] address rotation invariance, they overlook the impact of translation on place recognition.
- **Weather Conditions:** Laser signals exhibit varying behavior under different weather conditions. They attenuate less and travel farther on sunny days but decay significantly in rainy and foggy weather.
- **Perceptual Aliasing:** Distinct places in confined corridors may exhibit similar point cloud data, which introduces ambiguous interpretations.
- **Appearance Changes:** Long-term navigation applications [9], [10], [11], [36] often involve significant environmental changes, which leads to potential failures.
- **Sensor Characteristics.** Mechanical LiDAR [56], [78] produces point clouds in a format of multiple scan lines, resulting in vertical sparsity. Solid-state LiDAR [79] provides limited horizontal field-of-view (FOV) and requires specific considerations in the recognition process.

2.3 Relation to Previous Surveys

In recent years, there has been a proliferation of reviews on visual robotics technologies, addressing various topics such as place recognition [34], [35], [37], [38], localization [80], [81], tracking [82], [83], and SLAM [84], [85], [86]. While these reviews have made significant contributions to the progress of research in robotics and autonomous driving, they have regrettably neglected the technology of LiDAR sensors.

Cadena *et al.* [87] extensively reviews the current state of SLAM and delves into potential future directions. Yin *et al.* [88] provides a comprehensive place recognition survey encompassing cameras, LiDAR, radar, and joint sensors. However, the section dedicated to discussing LiDAR is relatively limited. Yin *et al.* [89] offers an informative overview of the recent progress and advancements in LiDAR-based global localization, while it merely represents a specialized branch of place recognition.

3 LPR TECHNIQUES: LOCAL DESCRIPTOR

The local descriptor was a compact representation of regions or points, capturing distinctive characteristics such as texture, color, density, or shape.

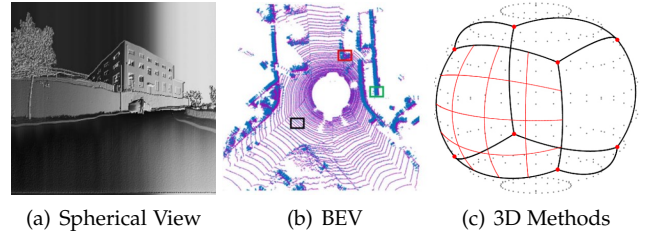


Figure 2: An illustration of handcrafted local descriptors. (a)-(c) were originally shown in [105], [47], and [3], respectively.

3.1 Handcrafted Methods

These methods usually extracted keypoints and then used local descriptors to describe their neighborhood. Table 1 contained a systematic summary of handcrafted local descriptors. According to the type of descriptors, they could be divided into 2D-based and 3D-based methods.

3.1.1 2D-based Methods

These methods projected a point cloud to a 2D image and built handcrafted local descriptors, then solved an image matching problem. According to their projection approach, these methods could be further divided into BEV and spherical view.

Spherical View. Steder *et al.* [103] projected the point cloud to a range image and computed key points based on a variant of the Laplacian of Gaussian (LoG). They subsequently extracted the local descriptor vector [107] and evaluated candidate transformations by re-projecting the key points. Although this approach yielded a superior recall rate, it required higher computation. Afterward, Steder *et al.* [15] extended the method [103] by combining normal aligned radial features (NARF) [108] and a bag-of-word (BoW) model to perform place recognition. Similarly, Zhuang *et al.* [104] extracted the speeded up robust features (SURF) [109] from the bearing angle image, but this method was mainly applied to dynamic indoor environments. As shown in Figure 2(a), Cao [105] aimed to improve place recognition search efficiency by projecting the point cloud onto a bearing angle image and using ORB [110] descriptors and DBow [111]. They also proposed a speed normalization approach and a 3D geometry-based verification algorithm. However, their image model might not perform well with viewpoint changes caused by lane shifts or seasonal variations. Shan *et al.* [106] utilized a point cloud with intensity information to create an intensity image and encoded ORB [110] descriptors into a BoW vector. They built a DBow [111] database for place recognition. Although the results were encouraging and not affected by changes in sensor attitude, this method did not account for motion distortion, which could affect its performance on high-speed platforms.

BEV. BVMATCH [52] used a multi-step process by projecting the point cloud to BEV images, extracting the maximum index map [112] of the Log-Gabor filter responses, and utilizing a BEV feature transform and BoW for place recognition. This approach provided relative poses using random sample consensus (RANSAC) [113] and could overcome sparsity and intensity distortion. In Figure 2(b), Luo *et al.* [47] detected the feature from accelerated segment

Table 1: Summary of handcrafted local and global descriptor methods. The methods in each sub-class were sorted according to their published year.

Methods		Year	Feature	Size	Metric	Code
Global Descriptor	BEV-based	SC [4]	Height	60×20	L0 Norm+Cosine Distance	✓
		ISC [44]	Intensity	60×20	Cosine Distance	
		LiDAR Iris [45]	Height	80×360	Hamming Distance	✓
		Shi <i>et al.</i> [90]	Height	60×20	Cosine Distance	
		WSC [91]	Height+Intensity		Cosine Distance+Euclidean Distance	
		SC++ [7]	Height	60×20	L1 Norm+Cosine Distance	✓
		RING [92]	Occupancy	120×120	Circular Cross-correlation	
		RING++ [93]	Height+Occupancy	120×120	Circular Cross-correlation	✓
		FSC [94]	Height+Intensity		F-Norm	
		PGHCI [65]	Height	40×20	JS Divergence+Pixel Values	
	Discretization-based	FreSco [95]	Height	20×120	L1 Norm+Cosine Distance	✓
		Ou <i>et al.</i> [96]	Density+Height	5×20×60	Cosine Distance	
		Magnusson <i>et al.</i> [97]	Shape		Euclidean Distance	
		DELIGHT [62]	Intensity	256	Chi-squared Test	
Local Descriptor	Point-based	Lin <i>et al.</i> [79]	Shape	60×60	Normalized Cross-correlation	✓
		Mo <i>et al.</i> [98]	Density+Intensity+Height	192+256+60×20	L2-Norm+Chi-squared Test	✓
		Cao <i>et al.</i> [99]	Context+Layout	360×180	Euclidean Distance	
		Z-Projection [60]	Normal	101	χ^2 Distance+Sørensen Distance	
	3D-based	Fast Histogram [46]	Height	80	Wasserstein Metric	
		M2DP [100]	Density	192	L2-Norm	✓
		C-M2DP [101]	Color+Shape	576	L2 Distance	
	2D-based	3DGestalt [59]	Height	32×10	Voting	
		NBLD [102]	Density	16×4×8	Voting	
		GLAROT-3D [3]	Orientation+Range	1880	Rotated L1 Norm	
		ISHOT [61]	Normal+Intensity	1344	Voting	✓
		Steder <i>et al.</i> [103]	Range+Curvature		Euclidean Distance	
		Steder <i>et al.</i> [15]	Range+Curvature	36	Manhattan Distance	

test (FAST) [114] keypoints on the BEV image, followed by constructing a histogram of orientations of principal normals (HOPN) descriptor using the principal normals of point clouds. They then introduced a voting-based algorithm for the consensus set maximization problem [115], which estimated a rigid pose from descriptor matches. This approach demonstrated superior localization capability and long-term robustness in large-scale scenarios.

3.1.2 3D-based Methods

These methods usually extracted 3D key points and descriptors. Inspired by the planar signatures geometrical landmark relations (GLARE) [116] and glare rotation invariant (GLAROT) [117], 3D Gestalt [59] analyzed the mean and variance of heights and presented a methodology for statistical modeling and analysis of keypoint vote distributions. This approach allowed for the automatic adjustment of crucial algorithmic parameters and facilitated the identification of place matches in sub-linear time. Neighbour binary landmark density (NBLD) descriptor [102] aggregated sparse triangulated landmarks into a compact signature by calculating the point density of each bin in cylinder space and comparing it with neighborhoods to describe the local feature. Although better suited for place recognition from sparse point clouds than 3D Gestalt [59], this method had its limitations as the appearance changes could not be arbitrarily strong. In Figure 2(c), GLAROT-3D [3] devised a histogram by encoding the relative positions of crucial points and measured a rotated F_1 norm to evaluate potential matching maps. While this method was effective in certain aspects, establishing connections between these keypoints proved to be computationally demanding. Intensity signature of histograms of orientations (ISHOT) [61] combined geometry and appearance by enhancing the SHOT descrip-

tor [118] with intensity and using a keypoint voting method, which was beneficial for cases where local displacement was the only estimation needed. However, detecting differences between sensors was difficult due to pre-processing of the sensor measurements, and a universal LiDAR intensity calibration standard was required.

3.2 Learning-based Methods

Similarly, learning-based methods were roughly categorized as 2D and 3D-based approaches.

3.2.1 2D-based Methods

DeLightLCD [119] utilized a deep and lightweight Siamese feature extraction module to extract distinctive features from 2D depth images and enhanced rotation invariance through a dual-attention-based feature difference module. Loop candidates were rapidly selected based on the ranging distance histogram. This method performed LCD without prior pose knowledge or predefined thresholds and excelled in parameter count and detection speed.

3.2.2 3D-based Methods

Zhou *et al.* [120] extracted local 3D deep descriptors [121] by a deep network and measured the overlap based on the metric error of registered points that were mutually nearest neighbors in the descriptor space. This approach accurately detected loops and estimated 6-DoF poses, particularly in cases with small overlaps.

3.3 Summary

Although local descriptors had been widely applied in tasks such as PCR and object recognition, they were not

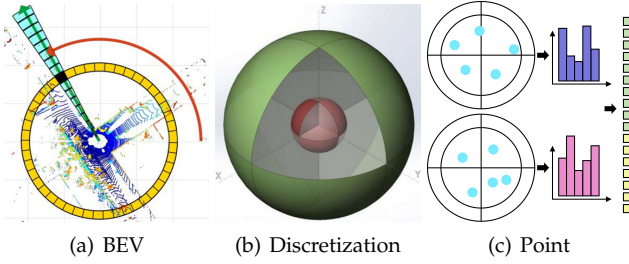


Figure 3: An illustration of handcrafted global descriptors.

commonly used methods for place recognition. There were mainly the following reasons:

- Viewpoint changes could affect the accuracy of 3D key points [122], rendering them unsuitable for matching. Moreover, they might not effectively handle data noise and object occlusions.
- The usage of 3D local descriptors [59], [102] could be challenging as it required dense point clouds, which was computationally expensive and might not work well with sensors like Velodyne VLP-16 [64] that produced sparse point clouds.
- While converting point clouds into images [103] could use mature image processing techniques, this resulted in the loss of geometric information, making it unsuitable for large-scale scenarios.

4 LPR TECHNIQUES: GLOBAL DESCRIPTOR

The global descriptor captured the overall features of a scene, providing a holistic view of the data rather than focusing on specific regions or points.

4.1 Handcrafted Methods

These methods usually used a single descriptor to describe the entire point cloud. Table 1 contained a systematic summary of handcrafted global descriptors. According to the type of space division, they could be divided into BEV-based, discretization-based, and point-based methods. Three representative methods were shown in Figure 3.

4.1.1 BEV-based Methods

These methods transformed the point cloud into the BEV representation. They could be further divided into Scan Context (SC) [4] family and pairwise matching.

SC Family. As shown in Figure 3(a), the pioneering work SC [4] partitioned the horizontal space into discrete bins while maintaining the points' maximum height to generate a 2D matrix descriptor. It then utilized the ring key to search for potential matches and conducted a column-wise comparison to identify the closest one. This method demonstrated promising performance but might fail when dealing with significant lateral offsets. Subsequently, researchers proposed a series of SC-based variant methods, which employed the polar and cart context [7], intensities [44], [91], frequency domain [95], local reference frame (LRF) [90], F-norm [94], and spatial binary pattern (SBP) [96] to enhance performance. Furthermore, certain studies [123],

[124], [125] had incorporated SC-based methods into the LCD module of LiDAR SLAM frameworks to enhance the performance of localization and map construction.

Pairwise Matching. Inspired by human iris signatures, LiDAR Iris [45] utilized LoG-Gabor filtering and thresholding operations to create binary signature images, then computed descriptor similarities using Hamming distance and applied Fourier Transform in the frequency domain for further analysis. This method improved matching and recognition efficiency, but generating signature images required more time. Polar grid height coding image (PGHCI) [65] assigned values to each grid based on height distributions and utilized the Jensen-Shannon (JS) divergence to compute the rotation transform. Descriptor similarities were estimated using two weighted distances. This method overcame the limitations of requiring the same types of sensors in mapping and localization by generating virtual scans. While the descriptor compensated for insufficient information due to the sparsity of far points, it might not be robust enough in scenes with similar structures, such as a building with multiple floors. RING [92] and RING++ [93] developed a groundbreaking framework for sparse place-based global localization, which utilized binary occupancy to represent point presence in the BEV grid and established a translation-invariant descriptor and an orientation-invariant metric for place recognition. It was impressive that this learning-free unified representation tackled all sub-tasks of global localization simultaneously.

4.1.2 Discretization-based Methods

These methods transformed the point cloud into a 3D discrete representation. They could be roughly divided into fixed and unfixed size-based methods.

Fixed-size Discretization. These methods divided the 3D space into fixed-sized sub-spaces. Magnusson *et al.* [97] mapped the point cloud to normal distribution transform (NDT) voxels and then proceeded to create a histogram based on the probability density function of the local surface. They then calculated the descriptor similarities through weighted Euclidean distances. While this approach did not yield a substantial improvement in the recall rate compared to visual methods, it provided evidence of the viability of NDT descriptors for place recognition. In [126], they extended this method to achieve place categorization using hierarchical k-means++ clustering [127]. Lin *et al.* [79] and Meng *et al.* [128] integrated the LCD module that divided the 3D space into cells and generated a 2D histogram by tallying the pitch and yaw feature directions. They then employed normalized cross-correlation to calculate the descriptor similarities. This approach was speedy, rotation-invariant, and performed well in detecting loops with precision and dependability. But the low correlation of vertical features in mechanical LiDAR affected vertical pose transformation estimation. Cao *et al.* [99] divided cylindrical space into wedge-shaped voxels to obtain projected images and generated a numerical descriptor by detecting contours and computing the spectrum energies. They combined Euclidean distance, approximate nearest neighbors (ANN) search, and temporal consistency check to achieve place recognition. The experimental results on three datasets

across seasons demonstrated that this method overcame challenging season changes and viewpoint shifts.

Unfixed-size Discretization. In Figure 3(b), DELIGHT [62] divided the support region into two concentric spheres and got non-overlapping bins by horizontal and azimuthal divisions. It computed intensity histograms for each bin and determined descriptor similarities by chi-squared tests. Interestingly, the descriptor could be local or global based on the descriptor’s outer radius and center point. However, this method relied heavily on point cloud density. Mo *et al.* [98] replaced LiDAR intensities with grayscale intensities and adapted DELIGHT [62] to a vision-based system for place recognition. However, this method required enough overlapped trajectory to accumulate 3D points.

4.1.3 Point-based Methods

These methods directly took the raw point cloud as input. Z-Projection [60] accumulated the angles between normals and z-axis into a histogram, then computed histogram similarities by the χ^2 and Sørensen distances. Fast Histogram [46] counted the height and distance information of the point cloud to create the histogram and then computed the histogram distance by Wasserstein metric. Both of the above methods transformed place recognition into histogram similarity calculation. They can achieve rotation invariance and overcome noises, but cannot provide the internal structure of the scene, which makes it less discernible for place recognition and may cause potential false positives. In Figure 3(c), M2DP [100] first projected the point cloud onto multiple 2D planes based on azimuth and elevation angle. It then divided each plane into separate bins and counted the number of points to generate a signature vector. These vectors were aggregated into a matrix and underwent singular value decomposition (SVD) analysis, creating the final descriptor by the first left and right singular vectors. This method’s ability to compute density signatures on multiple planes allowed for an accurate description and required fewer computational resources than other methods that used normals calculation, which was particularly effective when dealing with sparse point clouds. C-M2DP [101] further extended this method by adding color features.

4.2 Learning-based Methods

These methods applied learning techniques to obtain the global descriptor. According to their network architecture and model mechanism, they could be divided into five categories: point-based, discretization-based, classification-based, projection-based and fusion-based methods. Table 2 provided a overview of learning-based global descriptor.

4.2.1 Point-based Methods

These approaches directly processed LiDAR point clouds and utilized the inherent 3D spatial information. According to the network architecture for feature learning, they could be divided into pointwise multi-layer perceptron (MLP), point convolution, and graph representation. Figure 4 illustrated three representative point-based methods.

Pointwise MLP. As shown in Figure 4(a), the pioneering end-to-end work PointNetVLAD [12] combined PointNet [153] for local feature extraction and NetVLAD [41]

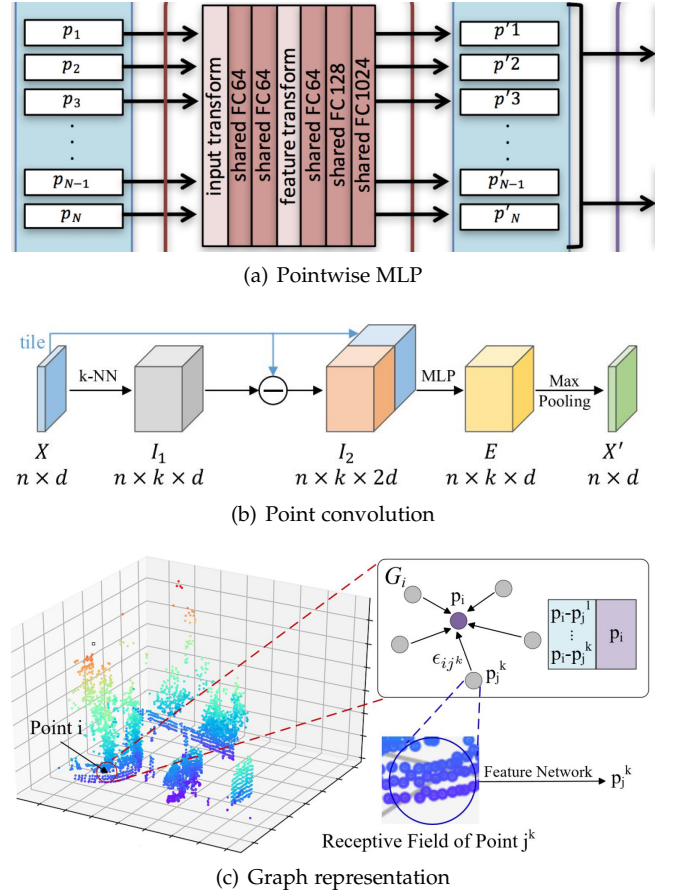


Figure 4: An illustration of point-based methods. (a)-(c) were originally shown in [12], [67], and [5], respectively

for global descriptor generation. This method employed metric learning [154] and introduced the lazy triplet and quadruplet loss functions to enhance the generality of global descriptors by maximizing differences among the hardest negatives in the training set. However, it suffered from PointNet’s limitations in capturing high-level features. PCAN [68] applied a sampling and grouping technique to extract multi-scale local contextual features and generated an attention-weighted global descriptor by a NetVLAD [41] aggregator. While this network prioritized task-relevant features, it did not effectively distinguish the significance of different neighbors or consider the contributions of individual features. SOE-Net [129] improved point-wise feature representation by integrating the orientation-encoding module with PointNet [153]. It introduced a self-attention unit to differentiate the importance of local descriptors. Additionally, this method introduced the hard positive hard negative (HPHN) quadruplet loss, which provided more versatile global descriptors than the commonly used lazy quadruplet loss [12], albeit with the need for pre-configuring the loss margin. LCDNet [130] introduced a shared feature extractor built upon the PointVoxel-RCNN (PV-RCNN) [155] architecture to extract point features. It then incorporated a place recognition head utilizing NetVLAD [41] to generate global descriptors and trained these descriptors by triplet loss. Additionally, a novel differentiable relative pose head based on unbalanced optimal transport theory estimated relative

Table 2: Summary of learning-based global descriptor methods organized according to the year of publication, backbone network, feature aggregator, descriptor size, loss function, and end-to-end (EtE) learning.

Method			Year	Backbone	Aggregator	Size	Loss	EtE
Point-based Methods	Pointwise MLP	Pointnetvlad [12]	2018	PointNet	NetVLAD	256	Lazy triplet and quadruplet	✓
		PCAN [68]	2019	PointNet	NetVLAD	256	Lazy quadruplet	✓
		SOE-Net [129]	2021	PointOE	NetVLAD	256	HPHN quadruplet	✓
		LCD-Net [130]	2022	PV-RCNN	NetVLAD	256	Triplet	✓
	Point Convolution	DH3D [69]	2020	FlexConv+SE block	NetVLAD	256	N-tuple	✓
		EPC-Net [67]	2022	PPCNN	VLAD	256	Lazy quadruplet	
	Graph	LPD-Net [5]	2019	PointNet	NetVLAD	256	Lazy quadruplet	✓
		DAGC [13]	2020	ResGCN	NetVLAD	256	Lazy quadruplet	✓
		SR-Net [131]	2020	SGC+SAM	NetVLAD	1024	Lazy quadruplet	✓
		vLPD-Net [132]	2021	LPD-Net, S-ARN	MinkPool		Joint loss	
		PPT-Net [133]	2021	Transformer	VLAD	256	Lazy quadruplet	
Discretization-based Methods	Sparse Volumetric	MinkLoc3D [134]	2021	FPN	GeM	256	Triplet margin	
		MinkLoc++ [135]	2021	ResNet18, FPN	GeM	256	Triplet margin	
		EgoNN [136]	2021	CNN	GeM	256	Triplet margin	
		TransLoc3D [137]	2021	Transformer	NetVLAD	256	Triplet margin	✓
		MinkLoc3Dv2 [138]	2022	FPN	GeM	256	Modified Smooth-AP	
		MinkLoc3D-SI [139]	2022	FPN	GeM	256	Triplet margin	
		SVTNet [8]	2022	Transformer	GeM	256	Triple	
	Dense Discretization	LoGG3D-Net [140]	2022	U-Net	O2P+ePN	256	Contrastive, quadruplet	✓
		SpoxelNet [141]	2020	CNN	NetVLAD		Lazy quadruplet	✓
		VBRL [142]	2020				Modality norm	
Projection-based Methods	Spherical View	HiTPR [143]	2022	Transformer	Max pooling	1024	Lazy quadruplet	
		NDT-Transformer [144]	2022	Transformer	NetVLAD	256	Lazy quadruplet	✓
		Yin <i>et al.</i> [145]	2017	DNN			Contrastive	
		MMCS-Net [146]	2022	Siamese CNNs	NetVLAD		Contrastive	✓
		SeqOT [147]	2022	Transformer	GeM	256	Triplet	✓
	BEV	OverlapTransformer [148]	2022	Transformer	NetVLAD	256	Lazy triplet	✓
		AttDLNet [149]	2021	DarkNet53	Max pooling	1024	Cosine similarity	
		OREOS [48]	2019	CNN			Triplet	
Fusion-based Methods	SCI [9]	SCI [9]	2019	LeNet			Categorical cross-entropy	✓
		DiSCO [66]	2021	U-Net		1024	Quadruplet, KL divergence	✓
	PIC-Net [150]	PIC-Net [150]	2020	Resnet50+PointNet	NetVLAD	512	Lazy quadruplet	
		CORAL [18]	2021	ResNet18, FPN	NetVLAD	256	Lazy quadruplet	✓
	Berneirer <i>et al.</i> [151]	Berneirer <i>et al.</i> [151]	2021	Spherical CNN			Triplet	✓
	Adafusion [152]	Adafusion [152]	2022	CNN	GAP	256	Pairwise margin	✓

transformations without prior information. This method combined the feature extraction capability of deep neural network (DNN) with transport theory algorithms for feature matching.

Point Convolution. These methods defined and applied convolution operations directly on the point cloud. DH3D [69] introduced a Siamese network that performs local feature detection, description, and global descriptor extraction in a single forward pass. Firstly, the network incorporated multi-level spatial contextual information and channel-wise feature correlations using flex convolution (FlexConv) [156] and squeeze-and-excitation (SE) [157]. It then utilized the N-tuple loss [158] for descriptor differentiation. Finally, this method aggregated attention-weighted local features into global descriptors using NetVLAD [41]. Experimental results demonstrated competitive performance in the global point cloud retrieval and local PCR, showcasing its favorable generality. In Figure 4(b), EPC-Net [67] first simplified original edge convolution [159] by the spatial-adjacent matrix and proxy points. It then extracted multi-scale local geometric features through stacked convolutional modules. Finally, a grouped VLAD network aggregated a low-dimensional global descriptor using grouped fully connected layers. Additionally, this method employed knowledge distillation to obtain a lightweight yet powerful model for efficient recognition. EPC-Net achieved excellent performance while significantly reducing computational memory and inference time.

Graph Representation. In Figure 4(c), LPD-Net [5] incorporated an adaptive local feature extraction and a graph-based neighborhood aggregation module. This approach

extracted ten types of local features, including curvature and density, using PointNet++ [160] and then employed a GNN for further processing. However, the computation of handcrafted features and the complex network architecture hindered the recognition efficiency. vLPD-Net [132] presented the first registration-aided adaptation network for point cloud-based place recognition. This approach employed LPD-Net [5] as a feature extractor and introduced a structure-aware registration network to combine geometry property and co-contextual information. Additionally, it utilized MinkLoc3D [134] for local feature aggregation and employed adversarial training to bridge the gap between synthetic and real-world domains. It demonstrated the effectiveness of the synthetic-to-real domain for outdoor point cloud-based place recognition. Dual Attention and Graph Convolution (DAGC) [13] introduced a dual self-attention module to distinguish task-relevant features and leverage the contributions of other points to generate representations. Additionally, it employed a residual graph convolution network (ResGCN) module to aggregate local features from neighboring points at multiple levels. This method improves descriptor generation by simultaneously considering the importance of points and features. PPT-Net [133] first utilized EdgeConv [159] on multi-scale KNN graphs to extract local embeddings and introduced grouped self-attention to learn spatial relationships between regions. A pyramid VLAD module then employed VLAD pooling on multi-scale feature maps to generate multi-scale global descriptors. Finally, the context gating mechanism adaptively weighted multi-scale global context information into the final global descriptor. Scene Recognition Network (SRNet)

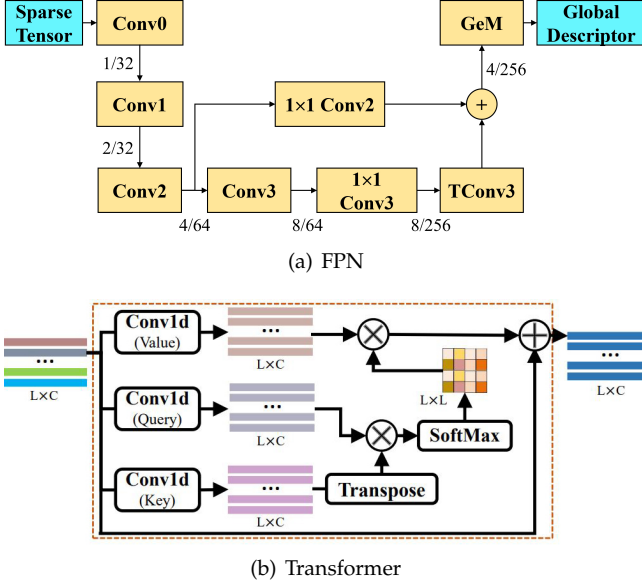


Figure 5: An illustration of two sparse volumetric representation methods.

[131] utilized stacked Static Graph Convolution (SGC) layers to extract local features. To mitigate the impact of movable noises, it incorporated a Spatial Attention Module (SAM) that redistributed attention to task-relevant areas during propagation. Additionally, SRNet introduced a Dense Semantic Fusion (DSF) strategy to compensate for the loss of shallow features during propagation and integrate multi-level features.

4.2.2 Discretization-based Methods

These methods usually converted a point cloud into the sparse volumetric or dense discretization representation.

Sparse Volumetric Representation. These methods partitioned the point cloud into voxels and utilized 3D CNNs on the volumetric representation to generate global descriptors. They could be roughly divided into feature pyramid network (FPN), transformer network, and other methods.

1) *FPN*. As shown in Figure 5(a), the pioneering work MinkLoc3D [134] initially employed sparse voxelization to quantize the point cloud, followed by feature extraction using a 3D FPN [161] architecture and generalized-mean (GeM) [162] pooling for global descriptor generation. This approach showcased a simple, elegant, and effective architecture, highlighting the potential of sparse voxelized representation and sparse convolutions for efficient 3D feature extraction. However, the voxelization procedure and hash map computation posed time-consuming challenges. MinkLoc3D-SI [139] extended MinkLoc3D [134] by utilizing the spherical coordinates and intensity values in a single 3D LiDAR scan. MinkLoc++ [135] introduced a multi-model descriptor extraction network to enhance MinkLoc3D [134]. It incorporated the efficient channel attention (ECA) [163] mechanism and utilized the first four blocks of ResNet18 [164] to generate a 2D feature map with 256 channels. This approach addressed the issue of modality dominance by extending the loss function with additional terms based on unimodal descriptors computed at intermediary processing

steps. MinkLoc3Dv2 [138] coupled MinkLoc3D [134] with channel attention blocks and introduced a modified smooth average precision (AP) [165] metric-based loss function. Additionally, it utilized multistage back-propagation [166] to allow using large training batches containing thousands of point clouds. Egocentric neural network (EgoNN) [136] increased the network depth of MinkLoc3D [134] and added ECA [163] to convolutional blocks to improve the performance on larger point clouds.

2) *Transformer Network*. TransLoc3D [137] initially employed sparse voxelization and 3D sparse convolution to process input points. It then applied a point-wise feature re-weighting scheme to re-weight features from multiple receptive scales by a learned attention map. Furthermore, external attention layers captured long-range contextual information, followed by a global descriptor aggregation using NetVLAD [41]. This method leveraged size-adaptive receptive fields and global contextual information, resulting in superior performance compared to state-of-the-arts (SOTAs), with substantial improvements on popular datasets. As shown in Figure 5(b), SVT-Net [8] proposed two types of transformers [167]: Atom-based sparse voxel transformer (ASVT) and cluster-based sparse voxel transformer (CSVT) on top of the 3D sparse convolutional network SP-Conv [168] to capture short-range local features and long-range contextual features, respectively. Although this method could generate descriptive descriptors with a shallow network architecture, it did not address challenges associated with sparse point clouds and complex situations.

3) *Other Methods*. LoGG3D-Net [140] first employed sparse U-Net [169] to embed each point into a high-dimensional feature space and introduced a local consistency loss to maximize feature similarity. It then aggregated local features by second-order pooling and differentiable Eigen-value power normalization to create a global scene-level descriptor. Finally, scene-level and local consistency loss worked jointly to optimize the network. This approach ensured feature consistency across revisits and exhibited superior performance in an end-to-end setting, operating in near real-time.

Dense Discretization Representation. These methods usually partitioned the point clouds as dense grids or voxels. They could be further divided into the transformer network, DNN, and other methods.

1) *Transformer Network*. HiTPR [143] first partitioned the point cloud into small cells by down-sampling and nearest neighbors search. Then, a short-range transformer extracted local features from the sampled center points within the cells. Next, a long-range transformer encoded global relations among the cells using transformer blocks with residual connections. Finally, an aggregation module comprising a linear transformation, batch normalization, activation function, and max-pooling operator aggregated a global descriptor. This approach enhanced the relevance of local neighbors and global contextual dependencies, showcasing its superior effectiveness. NDT-Transformer [144] compressed the point cloud into NDT cells and employed a transformer-based network to learn a global descriptor from the cell representations. The network comprised three stacked transformer encoders with shared linear stacks at the top and bottom, connected by a shortcut skip connection. This approach

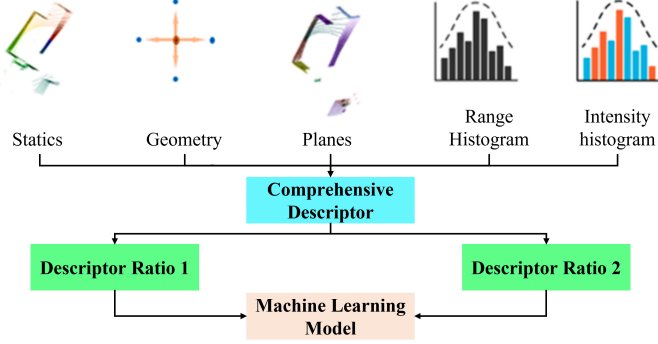


Figure 6: An illustration of classification-based methods. The figure was originally shown in [63].

achieved a balance between SOTA performance and runtime efficiency. It served as a valuable complement to NDT-based SLAM and MCL methods. However, its preprocessing step was unsuitable for online systems.

2) *DNN*. SpoxelNet [141] first voxelized the point cloud in spherical coordinates and represented voxel occupancy with ternary values. It then employed a neural network to extract structural features at different scales and generated a global descriptor by concatenating features from multiple directions. Finally, the output descriptor was compared to those from a pre-built reference map. This method effectively addressed occlusion and moving objects in crowded indoor spaces. However, the abstract features extracted by neural networks lacked interpretability.

3) *Other Methods*. Voxel-based representation learning (VBRL) [142] addressed long-term place recognition by jointly learning the importance of voxels and feature modalities using structured sparsity-inducing norms. It then integrated all features into a unified regularized optimization formulation.

4.2.3 Classification-based Methods

These methods usually trained a classifier to decide whether there was a loop. As shown in Figure 6, FastLCD [63] encoded multi-modality features, such as statistics, planes, geometry, range, and intensity, into a global descriptor. A supervised learning model then utilized descriptor ratios to detect loop closures. Finally, a double-deck loop verification strategy comprising cross-validation and post-verification rejected false positives. Habich *et al.* [170] encoded each LiDAR point cloud using a compact global descriptor [171] and performed the loop search within a variable radius based on the largest eigenvalue max of the position covariance. Loop events were subsequently predicted using an AdaBoost [172] classifier. While this method demonstrated positive results, the scan registration could encounter failures in case of numerous repeating elements, thus should add more restrictions.

4.2.4 Projection-based Methods

These methods projected a point cloud to the 2D image and designed a neural network to achieve place recognition. According to their projection approach, these methods could be further divided into spherical view and BEV. Figure 7 showed two representative projection-based methods.

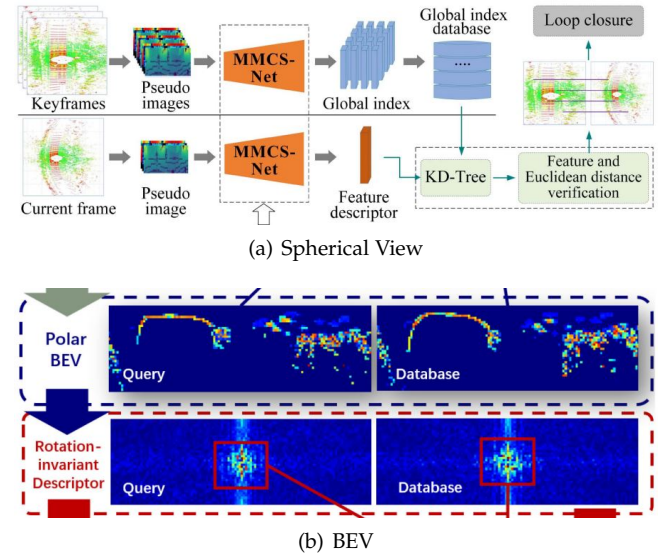


Figure 7: An illustration of projection-based methods. (a) and (b) were originally shown in [146] and [66], respectively.

Spherical View. These methods usually took the spherical projection image as the input. They could be further divided into three categories: Siamese network, transformer network, and 2D CNN only.

1) *Siamese Network*. Yin *et al.* [145] first converted the point cloud to a one-channel image using range distribution information and the ring structure in spherical coordinates. They subsequently employed a Siamese CNN to transform LCD into a similarity modeling problem. Finally, they combine Euclidean metric and kd-tree to enhance search efficiency. As shown in Figure 7(a), motivated by human-eye similarity judgment, MMCS-Net [146] introduces a multi-module cascaded Siamese CNN. It first incorporates a Siamese CNN with shallow-deep feature fusion and cascaded attention to process the generated pseudo images. A parallel graph neighborhood aggregation guided by key points encodes topology and depth for feature representation. Finally, a 1×1 convolutional layer compresses the aggregation feature into a 128-D vector. This method effectively encodes targeted features for challenging scenes and achieves a favorable compromise between effectiveness and efficiency.

2) *Transformer Network*. SeqOT [147] employed multi-scale transformer modules to generate sub-descriptors that fused spatial and temporal information from sequential LiDAR range images. A GeM [162] pooling was applied to exploit longer temporal information, fuse sub-descriptors, and create a lightweight global descriptor for each sequence. The yaw-rotation-invariant architecture ensured robustness to viewpoint changes and scan order, enabling reliable place recognition even in opposite driving directions. Overlap-Transformer [148] first utilized a modified OverlapNetLeg to extract features from range images. A transformer module then captured relative feature locations and global information across the entire range image. Finally, a global descriptor generator consisting of NetVLAD [41] and MLPs compressed the features into a yaw-angle-invariant global descriptor. This method achieved fast execution with less

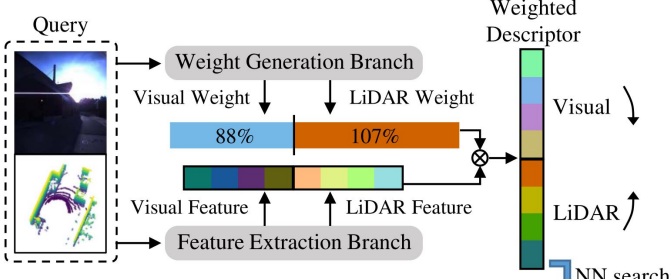


Figure 8: An illustration of fusion-based methods. The figure was originally shown in [152].

than 2ms per frame and demonstrated strong generalization across various environments without fine-tuning. Attention-based deep learning network (AttDLNet) [149] converted the point cloud to a range-based proxy representation and designed an attention network with four attention layers to capture long-range context and inter-feature relationships. This method combined KNN search with cosine similarity distance to search for loop candidates. The ablation study revealed that middle encoder layers demonstrated higher mean performance than other layers, while deeper layers performed better in oppo-direction revisits.

3) *2D CNN Only*. OREOS [48] employed a spherical projection model to project the point cloud onto a 2D range image. It then utilized 2D convolutional and max pooling layers to extract features, improving the descriptor performance via a triple loss function and strong negative mining strategy. This method efficiently computed the descriptor while preserving valuable information using handcrafted intermediate representation. It also allowed long-term 3-DoF metric global localization in outdoor environments.

BEV. Similarly, these methods usually took the BEV image as the input. They could also be divided into two categories: encoder-decoder network and 2D CNN only.

1) *Encoder-Decoder Network*. As shown in Figure 7(b), Differentiable scan context with orientation (DiSCO) [66] transformed features into the frequency domain and used the spectrum magnitude as the place descriptor. Specifically, it designed an encoder-decoder network to extract features in SC [4] descriptors and estimated relative orientation using Fourier-Mellin Transform and differentiable phase correlation. This lightweight network improved interpretability and enhanced the efficiency of the feature extractor.

2) *2D CNN Only*. Kim *et al.* [9] introduced a descriptor called scan context image (SCI), which normalized and extended SC [4] to three channels. They addressed robot localization on a grid map by formulating the place recognition problem as place classification with a convolutional neural network. Despite its robust year-round localization performance achieved within a single day of learning, this method remained susceptible to lateral offsets.

4.2.5 Fusion-based Methods

These methods integrated LiDAR and image features to enhance the descriptive capabilities of descriptors. CORAL [18] proposed a visual-LiDAR descriptor for bi-modal place recognition. It started by constructing a local elevation image and extracting multi-scale visual features

using ResNet18 [164] while capturing structural features through convolutional layers. A parameter-less projection layer established correspondences, followed by the feature representation by a fusion module. Finally, a combination of MLP and NetVLAD [41] enabled dimension reduction for the learned descriptor. Experiments demonstrated the generality of the network across different scenes and sensor configurations on cross-city datasets. As shown in Figure 8, Adafusion [152] designed an adaptive weighting visual-LiDAR fusion approach for place recognition. It calculated multi-scale spatial and channel attention from various layers of the feature extraction branch and combined them to obtain adaptive weights. These weighted features were subsequently concatenated into a global descriptor using global average pooling (GAP) [173]. PIC-Net [150] integrated point cloud and image features using an attention mechanism. It improved recognition performance in low-light conditions by transforming the night image into a daytime style [174]. The network utilized ResNet50 for extracting image features and PointNet [153] for point features. These features were subsequently processed through a spatial attention layer, channel attention layer, and global channel attention layer to obtain final feature representations. Bernreiter *et al.* [151] employed a spherical CNN [175], [176], [177] to learn a multi-modal descriptor for partially overlapping scenes. They estimated the power spectrum of each candidate and performed a correlation in the spherical harmonic domain to find the best match. This descriptor effectively generalized across various sensor systems for training, deployment, map building, and querying.

4.2.6 Summary

The global descriptor was currently the most popular place recognition method, which could provide information about the entire scene, unaffected by local changes. The progress of deep learning in 3D computer vision paved the way for data-driven methods in LPR. Several observations were summarized as follows:

For the handcrafted part:

- BEV [4], [7], [44], [91] had demonstrated good performance in flat structural environments, but there were three primary limitations: (1) If the z-axis of the LiDAR changes in the global coordinate system, poor results may be obtained because these methods assumed that the vehicle motion was locally planar. (2) Large lateral offsets might cause missed loops or failed re-localization. (3) Rotation matching could only compute yaw angles, and this method was prone to falling into a local optimum if used as the initial poses to iterative closest point (ICP) [178].
- Discretization-based methods [79], [97], [99] could describe the local surface using robust mathematical theories. However, increasing the resolution would significantly increase computational costs and memories.
- Point-based methods [46], [60], [100], [101] were the most basic global descriptor methods. However, they required expensive neighbor searching to establish topological relationships. Furthermore, some methods [100], [101] involved projection operations that

resulted in information loss and might cause potential false positives.

For the learning part:

- These methods delivered impressive efficiency and accurate recognition but heavily relied on ample training samples and extensive data cleaning. Real-world environments posed greater complexity than training datasets, introducing additional challenges such as noise, occlusions, and uncertainties in LiDAR measurements. Consequently, these methods might necessitate transfer learning for specific applications.
- Transformers [143], [144], [147], [148], [149] excelled at capturing long-range dependencies and contextual relationships, enabling reliable recognition in cluttered environments. However, their substantial computational demands constrained the batch size for metric learning.
- Sparse convolutional architecture [134], [135], [138], [139] could help produce informative local features while struggling to discriminate feature size in dynamic scenarios, and directly stacking convolution layers might overlook long-range contextual information.
- Point-based methods [5], [12], [13], [68], [69], [129] were permutation invariant and could handle unordered point clouds but lacked explicit capture of local spatial relationships. Classification-based methods [63], [170] assigned higher weights to informative features during training, emphasizing discriminative features. However, the specific contribution of each weak classifier to the overall prediction might be less interpretable.
- Projection-based methods [9], [48], [66], [146] had lower computational complexity and offered more interpretable results. However, they might suffer from information loss due to dimensionality reduction. Fusion-based methods [18], [150], [151], [152] harnessed the complementary strengths of different sensors. Nevertheless, achieving consistent data association in dynamic environments was still challenging.

5 LPR TECHNIQUES: SEGMENTS

Segments were meaningful region divisions characterized by similar geometric properties. Three representative methods were shown in Figure 9.

5.1 Handcrafted Methods

These methods divided the point cloud into sets of segments and extracted features from each segment for place recognition. Based on the processing approach of the segments, these methods could be classified into matching-based and similarity-based methods.

5.1.1 Matching-based Methods

These methods usually performed segment-based matching to find correspondences. They could be further classified into segmatch [72] family and other methods.

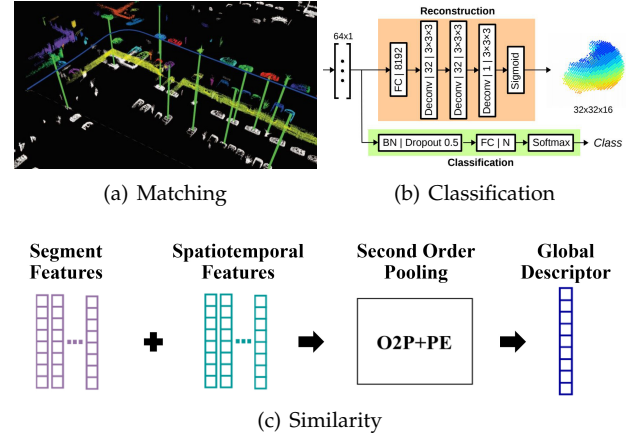


Figure 9: An illustration of three representative segment-based methods. (a)-(c) were originally shown in [72], [179], and [180], respectively.

SegMatch Family. In Figure 9(a), the pioneering work SegMatch [72] employed Euclidean clustering to partition the point cloud into segments and extracted eigenvalue-based features and an ensemble of shape histograms. It effectively identified potential correspondences using random forest and RANSAC-based geometric verification [113]. However, the computational efficiency of the method suffered due to its reliance on constructing a dense local map. Despite this limitation, SegMatch [72] demonstrated promising results and provided a reliable solution for matching point clouds. In [181], the authors extended their approach by proposing a region-growing-based incremental segmentation to track a single segment. In addition, researchers successfully integrated SegMatch [72] into traditional LiDAR SLAM [182] and multi-robot SLAM systems. Subsequently, researchers incorporate SegMatch [72] into traditional LiDAR SLAM and multi-robot system [183].

Other Methods. DL-SLAM [184] employed k-means to extract segments from the 2.5D heightmap and defined five descriptors to facilitate segment matching. However, the height invariant fails to hold in dynamic scenes, which necessitates segmenting the 2.5D heightmap into static and dynamic cells. RDC-SLAM [185] was a complete real-time distributed cooperative SLAM system that used DELIGHT [62] descriptor to perform the place recognition and obtain the alternative matches, then combined an eigenvalue-based segment descriptor, KNN search, and RANSAC-based verification [113] to refine relative pose. This system could fuse information from multiple robots accurately without prior knowledge. However, high-speed data collection might reduce accuracy because the brief connection time might not allow for a complete distributed graph optimization cycle. Gong *et al.* [186] introduced a two-level place recognition framework that leveraged a spatial relation graph to represent segments as nodes and their spatial relations as edges. The framework utilized an incremental BoW model to search for candidate graphs and evaluated their similarities using an improved spectral method. Experiments showed that this model-free method can effectively capture the general spatial relations between irregular clusters.

5.1.2 Similarity-based Methods

Seed [187] developed a segmentation-based egocentric descriptor for 3D point cloud scans, incorporating topological information into SC-based place recognition [4]. This method achieved translation and rotation invariance by utilizing the inner topological structure of segmented objects. However, performance degraded significantly in environments with less segmentation information.

5.2 Learning-based Methods

These methods typically employed learning techniques to achieve segmentation-based matching, classification, and similarity computation.

5.2.1 Matching-based Methods

Tinchev *et al.* [188] employed the convolution operation proposed in [189] to acquire an embedding space that could accommodate both urban and natural scenarios. They then estimated the match quality using probabilistic geometric validation. Unlike learning-based approaches, this method did not require a GPU at runtime, but it offered higher computational speed due to the network's customized design for the localization task. Tinchev *et al.* [190] encoded the geometric properties and point distribution of segments and extracted repeatable oriented key poses, which were matched with a reliable shape descriptor using a Random Forest. Nonetheless, the performance of segment matching might deteriorate when there was a significant change in the sensor's vantage point.

5.2.2 Classification-based Methods

These methods usually computed the category of segments by performing classification in the descriptor space. They could be further classified into segmap [179], [191] family and other methods.

1) *SegMap Family*. In Figure 9(b), the pioneering work SegMap [179], [191] incrementally clustered point clouds to create a global segment map. It employed segment-wise k nearest neighbors (KNN) retrieval using a data-driven descriptor extractor consisting of three convolutional and two fully connected layers, then assigned a classification score by a fully connected network. This method enabled high compression rates in environment reconstruction, facilitating large-scale 3D LiDAR SLAM while minimizing communication bandwidth between robots and the central computer. Subsequently, researchers successfully integrated SegMap [179] into LiDAR SLAM [192] and segment-based mapping framework [193].

2) *Other Methods*. Wietrzykowski *et al.* [194] proposed a DNN to bridge the gap between 3D segment-based and appearance-based methods, which learned visual context from synthetic LiDAR intensity images to enhance segment-based descriptors. They claimed that using the latest LiDAR technology with 128 beams and ambient images instead of intensity images could further improve performance. OneShot [64] was the first segment-based approach using only one LiDAR scan at a time. It employed a range image-based method [195] to extract segments and a custom-tailored neural network to extract LiDAR-Vision descriptors. Candidate matches were then verified using a geometric consistency test. Experiments showed that fusing image

features improved the descriptor retrieval rate by 17%-26% compared to using only LiDAR.

5.2.3 Similarity-based Methods

These methods extracted segment-based descriptors and computed their similarities. Deep Scan Context (DSC) [196] proposed an egocentric segmentation method to compute eigenvalues and centroids of segments. It then used a graph neural network (GNN) to aggregate these features into a descriptor for computing candidate similarity. This method was more efficient and robust than traditional Euclidean clustering in processing sparse point clouds. Experiments showed competitive performance and robustness against viewpoint changes and occlusion. In Figure 9(c), Locus [180] encoded topological and temporal information of segments to create a global descriptor using second-order pooling and nonlinear transformation. This method avoided global map construction and segment-wise KNN search, achieving robustness to viewpoint changes and occlusions.

5.3 Summary

Traditional point cloud descriptors relied on low-level properties [44], [46], [60], [62], [103], [104], [126] to encode the point cloud, but local descriptors lacked description ability, and global descriptors struggled with rotation and translation invariance. Fortunately, segment features offered a good compromise between the two. Several observations were summarized as follows:

- Segment-based methods [72], [179], [187], [191], [193] could reduce feature computation for place recognition by processing segments instead of the entire point cloud. However, some approaches relied on point cloud aggregation or map construction, which resulted in limited efficiency in dealing with large-scale environments.
- Segment-based place recognition had the potential to improve accuracy by incorporating geometric, color, and semantic information of segments. However, they required rich 3D geometry structures for segmentation, which might not always be available, thus limiting their applicability.
- Segment-based methods were known for their robustness to environmental changes, such as illumination, weather, and seasonal variations. However, they provided limited insights into underlying 3D structures, which could lead to poor segmentation performance in long-term localization and place recognition scenarios that involved many moving objects.

6 LPR TECHNIQUES: SEMANTICS

In the context of LPR, semantics actually represented a label or category. These methods divided the point cloud into different instances by learning-based semantic segmentation [197] and then performed semantic-level place recognition. Consequently, all of them were learning-based methods. According to the approach used for semantics association, these methods could be categorized into two main types: graph-based and graph-free methods. Two representative methods were shown in Figure 10.

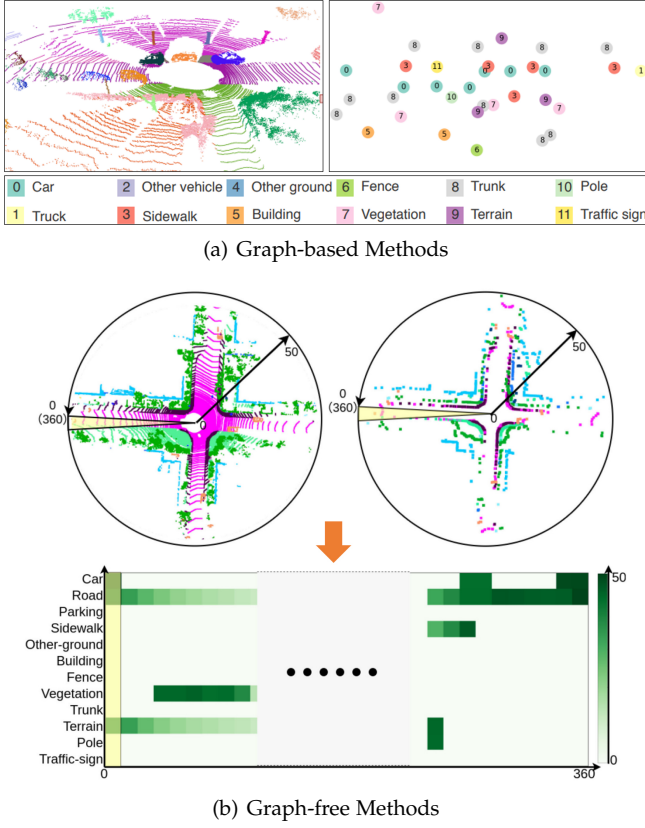


Figure 10: An illustration of two representative semantics-based methods. (a) and (b) were originally shown in [49] and [198], respectively.

6.1 Learning-based Methods

6.1.1 Graph-based Methods

These methods transformed the point cloud into a semantic graph to describe objects and their topology. They could be further divided into graph similarity and graph matching-based methods.

Graph Similarity. These methods computed the graph similarity to facilitate the comparison. X-view [199] generated random walk descriptors for each graph node and computed a similarity score by counting the number of identical random walks. This approach was general in semantic input and avoids high computation costs. Experimental results demonstrated that this method could globally localize aerial-to-ground and ground-to-ground robot data of drastically different viewpoints. As shown in Figure 10(a), SGPR [49], [51] presented a novel semantic graph-based approach for place recognition, which represented semantic categories and centroids of points as nodes and captured node feature relations using edges. It developed a GNN-based graph network consisting of node embedding, graph embedding, and graph-graph interaction to compute graph similarity. Extensive evaluations demonstrated the approach’s robustness to occlusion and viewpoint changes, particularly for reverse loops.

Graph Matching. These methods usually performed a graph matching. GOSMatch [50] proposed an object-based place recognition approach in urban environments, which searched candidates using graph descriptors and calculated

one-to-one correspondence using vertex descriptors, then identified loop closures by combining RANSAC [113] and SVD. Experiments showed the potential of using the relative position relationship between objects to improve reliable LCD. BoxGraph [200] represented scenes as compact semantic graphs where each vertex stores object shapes and reduced place recognition to an optimal vertex assignment problem. This method applied the bounding box as appearance embeddings of vertex entities and extended it for pose estimation. Although experiments proved that pose estimation performance was competitive with geometry-based methods, this method heavily relied on the accuracy of semantic segmentation.

6.1.2 Graph-free Methods

These methods avoided building graph representation and could be classified into semantics descriptors and other methods.

Semantics Descriptors. Semantic Scan Context (SSC) [71], [201] enhanced SC [4] by utilizing semantics [197] instead of height information. This method also employed a two-step global semantic ICP to improve matching accuracy. Object Scan Context (OSC) [202] improved on SC [4] by constructing the descriptor around uniformly distributed objects (e.g., street lights and trash cans) and using a bubble filtering algorithm to select matching correspondences. This approach made the descriptor independent of LiDAR’s position and overcame the issue of distant point clouds. Seq-NDT [203] extended the NDT-based histogram descriptor [204] by incorporating semantic information and used the kullback-leibler (KL) divergence to measure similarity. This method was resilient to initial registration error but required a dense global map. However, the accuracy of pose estimation was constrained by the map resolution. In Figure 10(b), RINet [198] introduced a new rotation equivariant global descriptor that integrates semantic and geometric information and then uses a lightweight siamese network with convolution, downsampling, and attention mechanism to compute descriptor similarities. This method prioritizes scene learning over point cloud orientation and is highly efficient, allowing for deployment on resource-constrained platforms.

Other Methods. Bernreiter *et al.* [205] employed multiple hypothesis trees to establish the probabilistic data association of semantic observations based on location, instance, and class. This method enabled precise localization in complex urban environments by exploiting the semantic co-visible maps. OverlapNet [70], [206] incorporated depth, normal, intensity, and probability distribution over semantic classes to predict the overlap and yaw angle between LiDAR pairs by a siamese neural network. The authors also applied this method to 3D LiDAR global localization [207]. However, inferring the complex network backbone and normals calculation resulted in poor efficiency. PSE-Match [208] introduced a parallel semantic embedding network to learn viewpoint-invariant spherical representations with a divergence learning metric. This method overcame local translation and orientation differences through spherical convolution, providing stable consistency in complex environments and avoiding disturbance from dynamic objects. SC-LPR [209] was a spatiotemporal place recognition method that

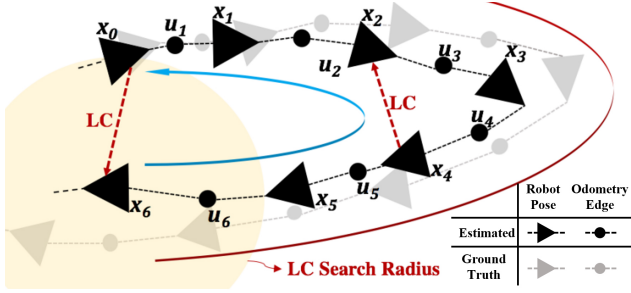


Figure 11: An illustration of odometry-based methods [211].

fused temporal and topological information using gated recurrent unit (GRU) and EdgeConv++. It combined Cosine Tensor Network with a neural tensor network (NTN) [210] to predict similarity scores. The method was independent of prior poses and achieved accurate predictions and superior recognition performance.

6.2 Summary

Humans perceived surroundings by identifying objects and their topological relationships. Inspired by this, semantic-based methods used pre-defined knowledge databases to assign categories to each object. However, these methods were still relatively new and immature because they need advanced semantic segmentation technology. Several observations were summarized as follows:

- Graph-based methods [49], [50], [51], [200] simplified the comprehension of point clouds but had three limitations: (1) They might lose certain features, such as object size. (2) Inability to distinguish between parts of the same category could lead to information loss. (3) Computing metrics between two graphs was NP-complete, making it difficult to calculate the exact distance in a reasonable time.
- Semantic labeling [197] yielded more interpretable and intuitive results than solely using geometric features. It was also more resilient to occlusion and viewpoint changes, particularly in reverse LCD. Nevertheless, the available predefined semantic labels in test datasets were limited and did not encompass numerous categories in real-life scenarios.
- Using objects and their topological information could improve recognition accuracy in dynamic or cluttered environments. These methods relied heavily on the outcomes of semantic segmentation, which could lead to poor performance in diverse scenarios. Despite these challenges, semantics-based methods showed promise in applications where traditional methods might be insufficient.

7 LPR TECHNIQUES: TRAJECTORY

These methods utilized data association between current and recent historical scans for place recognition. According to the usage methods of historical data, they could be divided into two categories: odometry-based (handcrafted) and sequence-based (learning) methods.

7.1 Handcrafted Methods

7.1.1 Odometry-based Methods

These methods directly detected loop closures based on the front-end odometry of the SLAM system. They could be further divided into four categories: naive Euclidean distance, overlap ratio, and PCR-based test.

Naive Euclidean Distance. Rottmann *et al.* [212] employed a wall-following technique to gather odometry data and utilized a piecewise orientation function to compare the shaped neighborhood similarities of poses and identified corresponding vertices. This approach was not restricted to any specific environment structure, such as rectilinear or linear features, and could accommodate low-range or binary sensors without making any additional assumptions. LIO-SAM [53] created a LiDAR inertial odometry framework that integrated a naive Euclidean distance-based place recognition with a global factor graph for accurate robot trajectory estimation. This approach was ideal for multi-sensor fusion, as it can seamlessly incorporate new sensor measurements as additional factors. Wen *et al.* [213] introduced a pipeline for multi-sensor calibration and mapping, which adopted a 20s timestamp interval and detected loops by measuring the Euclidean distance between two frames' origins in the world coordinate system. This method effectively resolved point misclassification issues by normalizing distances during feature point smoothing calculation and efficiently generated colored point clouds with centimeter-level accuracy.

Overlap Ratio S4-SLAM [214] contained a heuristic location-based LCD that stored historical poses through a kd tree and evaluated candidate loops based on overlap rate. This method balanced real-time and accuracy and remains robust, even with few feature points and high moving speed. Mendes *et al.* [215] used an overlap criterion to create new keyframes and a graphical model layer on top of LiDAR odometry to reduce overall drifts through graph-level loop closing. Hard rejection based on normals angles prevented unexpected drifts from vegetation but might cause overlap estimation to fall below the threshold quickly.

PCR-based Test These methods usually validated candidates by PCR techniques, such as standard ICP, point-to-line/plane ICP, and generalized ICP (GICP).

1) *Standard ICP.* IN2LAAMA [216] created an offline probabilistic framework for localization, mapping, and extrinsic calibration. The system identified loop closures using estimated poses and validated candidates with an optional ICP [178] test. Although capable of handling motion distortion without an explicit motion model, the current implementation lacked real-time functionality.

2) *Point-to-Line/Plane ICP.* The pioneering work Lego-LOAM [56] calculated odometry poses through a two-step Levenberg-Marquardt optimization based on planar and edge features. It then compared historical scans using pose constraints and refined the transformation using ICP [178] to correct accumulated errors. This method was the pioneering work to incorporate LCD into LiDAR SLAM, making it well-suited for long-duration navigation tasks. However, it heavily relied on the ground segmented from the online scan. LILO [54] devised a LiDAR-IMU system

with loop closure optimization, utilizing KD-tree sorting to locate the nearest frame and ICP [178] for relative pose computation. While this system could correct trajectories and historical poses, its primary focus was redundant point removal and map construction. LipMatch [217] created a plane graph for each keyframe and used the geometric properties of the planes and their relative positions to identify loop closures. It also boosted the robustness of ICP [178] by utilizing matched planes between keyframes. While it delivered comparable results to other methods in urban environments, it might falter in situations with few planar features or if the planar features could not be associated when the viewpoint changed. LiTAMIN [218] proposed a matching-based SLAM that approximates local geometry using normal distributions and detected loop closures by combining stable ICP [178] with an intuitive weighting method. Experiments showed that it reduced the impact of incorrect loop closure constraints and had comparable computational efficiency to LeGO-LOAM [56]. LiTAMIN2 [219] further incorporated KL-divergence to expedite registration without sacrificing accuracy. However, determining the optimal parameter settings for diverse environments necessitated further research.

3) *GICP*. As shown in Figure 11, LAMP [211] developed a multi-robot LiDAR SLAM system for challenging subterranean environments that utilized GICP [220] to register nearby scans and proposed an incremental consistent measurement (ICM) set maximization [221] to reject outlying loop closures. Although this method may miss loop closures due to odometry initialization, it can still compute many putative loops. LAMP 2.0 [222] introduced a scalable multi-robot front-end that supported inter and intra-robot LCD using Euclidean distance, point-to-plane ICP, and a graph neural network. This method computed the relative transform and filtered poor matches by combining TEASER++ [223] and GICP [220]. While this method performed well in experiments with up to four robots, its centralized architecture may not scale to large robot teams. SPC-SLAM [224] introduced an LCD module that leverages the geometric-rigidity-constant assumption between sub-maps using g2o [225]. The module compared current and past poses and then computed a submap registration score [220] to confirm loop closure. This approach effectively addressed the challenge of high-precision mapping in global navigation satellite system (GNSS)-denied environments using sparse point cloud data.

7.2 Learning-based Methods

7.2.1 Sequence-based Methods

These methods usually located the best match by sequence matching. The pioneering work SeqSLAM [227] utilized visual feature similarity comparisons over time to integrate sequence information and calculated the best candidate match within each local sequence. This method delivered exceptional performance across extreme environmental changes and provided fresh insights for LiDAR-based solutions. They could be further divided into scan and submap matching-based methods.

Scan Matching. As shown in Figure 12, SeqLPD [226] employed LPD-Net [5] for global descriptor extraction and

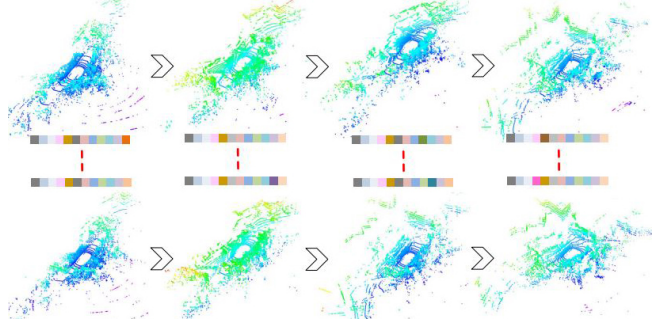


Figure 12: An illustration of sequence-based methods [226].

selected super keyframes based on feature space distribution. It combined super keyframe-based coarse matching with the local sequence fine matching to improve detection accuracy and efficiency. This method achieved advanced performance without relying on odometry data. The trained model could be directly applied in real-world scenarios without additional training, facilitating practical applications.

Submap Matching. Chen *et al.* [228] integrated LPD-Net [5] with sequence-based matching [227] for LCD but introduced a plane-driven sub-maps matching algorithm to close loops, which computed relative transformation by sampling environmental and ground plane pairs and employed interval stabbing for translation search. Experimental results demonstrate the algorithm's determinism and nearly real-time computation capabilities. SphereVLAD [6] extracted orientation-equivariant local features through a spherical convolution module under multi-layer spherical perspectives and employed a coarse-to-fine sequence matching to improve place recognition accuracy. This method was effective for changing viewpoints and large-scale SLAM problems. However, the computational expense of transitional sequence matching limited its direct application in real-world scenarios. FusionVLAD [229] proposed a multi-view fusion network that encoded top-down and spherical-view features from the local map, enhancing feature combination through a parallel fusion module for end-to-end training. This approach was well-suited for large-scale mapping tasks with limited computation resources. However, it might not perform well in confined spaces where LiDAR maps were sparse, limiting the generation of rich textures from top-down or spherical views. Additionally, RANSAC-based plane fitting [113] for top-down view generation was only suitable for structured ground. Yin *et al.* [55] employed SphereVLAD [6] to obtain viewpoint-invariant place descriptors from spherical representations and devised a fast coarse-to-fine sequence-matching mechanism using a particle filter framework. This method effectively balances matching accuracy and efficiency and exhibits high robustness against orientation and translation discrepancies. Additionally, the lightweight network structure permits lower-cost robots to perform large-scale localization tasks.

7.3 Summary

Traditional frame-to-frame comparison methods yielded an intuitive similarity score but intended to degrade in closed,

symmetric, and dynamic environments. The trajectory-based approaches incorporated both spatial and temporal information to address this limitation. Two observations were summarized as follows:

- LiDAR SLAM systems [211], [224] employed a straightforward LCD method based on pose proximity, followed by PCR [178] to calculate relative transformations. Although these methods yielded satisfactory results for short trajectories, two limitations persisted: (1) Cumulative errors compromised the reliability of odometry poses in large-scale scenarios. (2) The local optimality of ICP-based PCR [178] impeded the integration of loop constraints into global optimization.
- Sequence-based methods were versatile as they can effectively combine with various place recognition techniques, including local and global descriptors [55], [226], semantics, and segments. While visual sequence-based methods had been well-studied, LiDAR-based approaches were still in their early stages of development. Furthermore, the expensive calculations required for matching and feature fusion restricted their practical applicability.

8 LPR TECHNIQUES: MAP

These methods accomplished LCD by establishing a correlation between online scans and the map. Figure 13 illustrates four representative maps.

8.1 Handcrafted Methods

Based on the timing of map construction, these methods could be divided into two categories: offline map-based and online map-based methods.

8.1.1 Offline Map-based Methods

These methods generated a prior map before the system was activated, which remained unaltered as the vehicle moved and ensured vehicles move within its boundaries. According to the type of map, these methods could be further divided into five categories: feature, probability, point cloud, grid, and mesh.

Feature Map. Dong *et al.* [10] introduced a range image-based pole extraction approach. In the mapping phase, they extract poles from range images to build a global map. In the localization phase, Monte Carlo Localization (MCL) updated the particle's importance weights by matching online and map poles. Experimental results showcased accurate pole extraction in diverse environments, resulting in enhanced performance for long-term localization tasks. Shi *et al.* [230] used RANSAC [113] and Euclidean clustering to extract walls from the offline map and online scans. They then applied point-to-point and point-to-line distance constraints to compute the vehicle's global transformation. While this method improved computation efficiency slightly, it was unsuitable for wallless scenarios like cities and highways.

Probability Map. Schmiedel *et al.* [22] introduced the IRON descriptor, which characterized surface patches based on curvature and object shape within NDT maps. This method matched descriptors between online scans and the

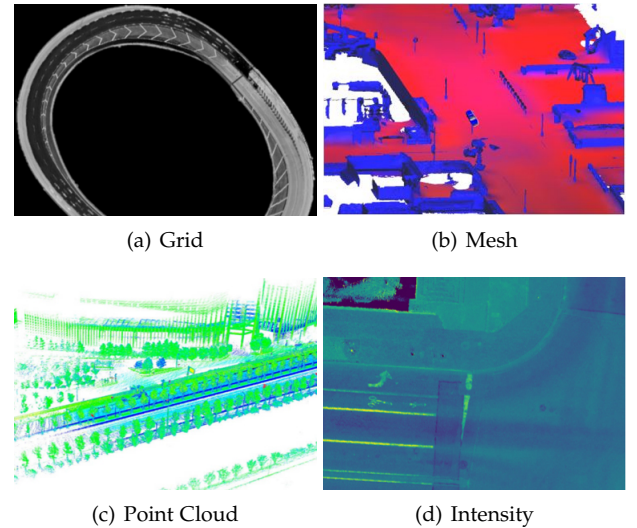


Figure 13: An illustration of four types of maps. (a)-(d) were originally shown in [232], [75], [77], and [233], respectively.

global map, applied RANSAC [113] for outlier detection, and evaluated the matches using a normalized inlier ratio. The integration of the keypoint data structure within the descriptor facilitated real-time applications. Additionally, transforming points into discrete NDT cells enhanced its clutter resistance.

Point Cloud Map. Xu *et al.* [73] introduced a cross-section shape context (CSSC) descriptor that utilized elevation and point density weights to describe the spatial distribution. They then searched candidates by a kd tree and enhanced recognition performance by combining two-stage similarity estimation and the nearest cluster distance ratio. Finally, they proposed a selective generalized ICP (SGICP) method for localization and pose calculation, eliminating unnecessary covariance matrix computation. While overcoming non-convergence issues in filter-based approaches, this method could not meet real-time requirements. Shi *et al.* [231] proposed an efficient template descriptor-based global localization method, which can run at 100 frames per second (FPS) on a single-thread central processing unit (CPU). They created an offline map database with a kd tree to simulate vehicle orientations and developed a binary loss function to improve localization accuracy.

Grid Map. In Figure 13(a), Aldibaja *et al.* [232] transformed LiDAR scans into image-like road surface representations, incorporating elevation and irradiation information. They used a shared ID-based XY correlation matrix to represent loop-closure events among all map nodes, enabling scalability for large-scale map processing and detection of map-combiner events independent of driving trajectory and LiDAR calibration. Incorporating elevation maps also improved the detection of multilayer road structures.

Mesh Map In Figure 13(b), Chen *et al.* [75] employed Poisson surface reconstruction to generate a prior mesh map. They then utilized the discrepancy between LiDAR range images and synthetic views of the mesh map to formulate an observation model for an MCL framework. This method demonstrated strong generalization across various

LiDAR sensors, did not need new training data in different environments, and could operate online at the sensor frame rate.

8.1.2 Online Map-based Methods

These methods dynamically constructed and updated an online map of the surrounding environment as the vehicle navigated within unknown terrain. In Figure 13(c), Multi-metric linear least square (MULLS) [77] introduced a scanline independent LiDAR SLAM that utilized TEASER [223] for loop verification between sub-maps and employed map-to-map ICP [178] to enhance inter-submap edges with precise transformations. While this method ensured low drift and high map quality, some closures might go undetected due to the high computational cost for each alignment. Continuous-time ICP (CT-ICP) [57] projected a local map onto an elevation image and extracted rotation-invariant 2D features. It then obtained an initial 2D transformation using RANSAC [113] in two feature sets and computed a 6-DoF pose by ICP [178] to get candidate loop closures. However, this method required the vehicle’s movement to be horizontal. Liu *et al.* [234] introduced a real-time 6D SLAM method for large-scale natural terrains, which combined rotation histogram matching with a branch and bound search-based ICP [178] algorithm to achieve real-time LCD. Real-world experiments demonstrated a significant reduction in odometry pose accumulation error and excellent performance in 3D mapping.

8.2 Learning-based Methods

Similarly, these methods were divided into offline map-based and online map-based methods.

8.2.1 Offline Map-based Methods

According to the type of map, these methods were roughly divided into three categories: intensity, point cloud, and node.

Intensity Map. In Figure 13(d), Barsan *et al.* [233] addressed localization using a deep recursive Bayesian estimation approach. They embedded LiDAR intensity maps and online scans into a joint space, employing efficient convolutional matching to compute the vehicle’s position. This method achieved centimeter-level accuracy and demonstrated robustness by working with uncalibrated data and generalizing across the different LiDAR sensors.

Point Cloud Map. These methods were further divided into MCL, kd tree, and pointwise MLP.

1) *MCL*. LocNet [19], [235] introduced a semi-handcrafted DNN and an MCL framework for global metric localization, which employed a Gaussian mixture model to model multiple hypotheses of place recognition results. This method leveraged the learned representations and vehicle poses to construct a prior map, achieving high accuracy and efficiency for long-term localization. Sun *et al.* [236] combined the efficient inference of a deep deterministic model with the rigorous geometry verification of a Bayes-filter-based approach to address the non-conjugacy issue between Gaussian and MCL. Experimental results demonstrate that this method achieved centimeter-level precision

while greatly faster than the traditional MCL method, making it suitable for large-scale real-world localization problems.

2) *Kd Tree*. Jin *et al.* [237] utilized the D3feat descriptor [238] and introduced a self-supervised detector loss for feature matching. They employed a kd tree to store map descriptors and proposed a coarse-fine voting mechanism and a two-phase search strategy to enhance search efficiency. Experimental results demonstrate the method’s significant reduction in robot walking time in unknown environments, ensuring robot safety.

3) *Pointwise MLP*. L3-Net [26] first extracted key points via linearities and scattering defined with eigenvalues. It then employed a mini-PointNet for feature descriptor extraction and regularized the cost volume by 3D convolutions. Finally, matching probabilities were computed for optimal estimation while deep recurrent neural networks (RNNs) captured temporal motion dynamics. This method achieved comparable localization accuracy to previous SOTA approaches and was suitable for industrial use and multi-sensor fusion frameworks. Retriever [14] utilized compressed representation and attention-based aggregation for place recognition in the compressed point cloud maps. An encoder extracts a compact task-agnostic feature representation, refined by a feature propagation network for task-specific representation. A perceiver-based attention module aggregates the features into a global descriptor. Experiments demonstrated the benefits of working directly on the compressed representation, bypassing compute-heavy decompression, and improving computing efficiency.

Node Map. S4-SLAM2 [239] built the node map comprising point cloud data, feature vectors, and location information. Subsequently, it extracted geometric and statistical features to create multi-modal descriptors and classified loop closures with a random forest classifier. Despite demonstrating effectiveness and feasibility in experiments, the method suffered from time-consuming loop verification and required large memory to store the node cloud map.

8.2.2 Online Map-based Methods

Similarly, these methods were roughly divided into surfel-based and grid map-based methods.

1) *Surfel Map*. SuMa [240] and SuMa++ [74] employed range images and surfel-based maps for data association, detecting candidate loops through a combination of radius search and frame-to-model ICP registration [178]. They then verified loops by tracking poses in both active and inactive maps. These methods ensured robust detection, even with low overlap, and yielded precise registration results and globally consistent maps.

2) *Grid Map*. Yin *et al.* [241] implemented place recognition using low-dimensional feature matching rather than geometry matching. Specifically, they generated a BEV map from the local occupancy map, considering vehicle motion errors. Furthermore, they introduced an additional GAN [242] with conditional entropy reduction to enhance unsupervised feature learning for long-term recognition applications.

8.3 Summary

Maps [26], [231], [236] had been widely used in robot localization and path planning as they offered precise and detailed representations of the environment. Remarkably, map-based methods excelled in recognizing topologically similar localization, providing pose information, and recovering kidnapped robots effectively. Several observations were summarized as follows:

- Map representations provided global consistency to help reduce localization errors. However, the substantial memory requirements of maps contributed to time-consuming loading, communication, and processing.
- Map-based methods could overcome noise and partial occlusions, ensuring robust recognition even in challenging scenarios. However, the significant density difference posed difficulties in registering online scans to maps.
- A robust prior map facilitated long-term robot localization in a consistent environment. However, significant environmental changes could cause the existing map to be outdated, resulting in localization and recognition errors.

9 LPR TECHNIQUES: OTHER METHODS

InCloud [243] introduced incremental learning for LPR, which distilled the angular relationship between global representations to preserve the complex structure of the embedding space between training steps. This approach effectively tackled the issue of catastrophic forgetting, enabling models to be updated with new domains without the need to retrain the network on all legacy data. Granström *et al.* [171] encoded the point cloud using geometry features and range histograms, followed by using a trained AdaBoost [172] classifier to detect loops. While achieving high precision and recall rates, this method required the ordered point cloud.

10 BENCHMARKING

In this section, we summarized existing datasets and evaluation metrics while comparing existing methods on public datasets.

10.1 Datasets

A large number of datasets had been collected to evaluate the performance of LPR methods. Table 3 provided a summary of these datasets. Their characteristics were summarized as follows:

- **Long-term Collection.** [246], [247], [252] repeatedly gathered the same scenario along similar routes in different seasons or times.
- **Multi-modal Data.** In addition to LiDAR sensors, radar was used in [250], [252] and cameras were mounted in [148], [208], [244], [245], [246], [247], [251], [252], [253]. Semantic information was also available in [249].
- **LiDAR Sparsity.** These datasets covered various density LiDAR sensors, such as mechanical 16-line

[248], [251], 32-line [246], [252], 64-line [244], [245], and 128-line LiDAR [94], as well as solid-state LiDAR [79].

- **Viewpoint Change.** In addition to same-direction revisits, [94], [99], [146], [148], [245], [246], [247], [248], [249], [250], [251], [252], [253] contained reverse loops.
- **Scenario Diversity.** These datasets were generally divided into two categories: indoor and outdoor datasets. Outdoor datasets were the most widely used, mainly including campuses [246], highways [248], rural areas [245], cities [251], and riversides [250].

10.2 Evaluation Metrics

Different evaluation metrics had been proposed to test LPR methods, summarized as follows:

- **Revisit Criteria:** A distance threshold was defined before evaluation to determine whether the query and candidate belonged to the same place.
- **Precision-recall (PR) Curves** [111]: This curve measured the relationship between precision (P) and recall (R) under different threshold parameters. P measured the ratio of correct matches to the total of predicted positive instances, while R quantified the proportion of real positive cases correctly identified as positive matches:

$$P = \frac{TP}{TP + FP} \quad (3)$$

$$R = \frac{TP}{TP + FN} \quad (4)$$

where TP , FP , and FN represented true positive, false positive, and false negative, respectively.

- **Area Under the PR Curve (AUC)** [9], [70]: It reflected the discrimination power of a place recognition method and a larger AUC meant more places were recognized with fewer errors. However, it did not retain any information regarding the features of the original PR Curve.
- **Recall @Top-N:** It evaluated the accuracy of place recognition methods in identifying the correct places among the top-k retrieved matches. A higher value indicated better performance. TOP 1% [52] and TOP 1 [92] were the two most frequently used metrics.
- **F_β Score:** It was the harmonic mean of precision and recall. A high value indicated the system strode a good balance between them as follows:

$$F_\beta = (1 + \beta^2) \times \frac{P \times R}{\beta^2 P + R} \quad (5)$$

where P and R represented precision and recall, respectively. β was a parameter that determined the weights of recall and precision. F_1 score [49], [63], [70], [71], [180], [186], [196], [200] was the most frequently used metric:

$$F_1 = 2 \times \frac{P \times R}{P + R} \quad (6)$$

Table 3: A summary of existing datasets for LPR. GT and LT represented the ground-truth and long-term, respectively. S and O represented the same and oppo-direction loop, respectively.

Year	Name	Sequences	Trajectory (KM)	Type	Sensor Modity	Model of LiDAR	Loop	GT	LT	Public
2009	Hannover2 [97]	1	1.24	Outdoor	LiDAR		S+O	✓		✓
2010	Freiburg [103]	1	0.723	Outdoor	LiDAR	SICK LMS	S	✓		✓
2011	Ford Campus [244]			Outdoor	Camera+LiDAR	Velodyne HDL-64E		✓		✓
2012	KITTI Odometry [245]	22	39.2	Outdoor	Camera+LiDAR	Velodyne HDL-64E	S+O	✓		✓
2016	NCLT [246]	27	147.4	Indoor+Outdoor	Camera+LiDAR	Velodyne HDL-32+Hokuyo UTM-30LX+Hokuyo URG-04LX	S+O	✓	✓	✓
2017	Oxford RobotCar [247]	> 130	>1000	Outdoor	Camera+LiDAR	SICK LD-MRS+SICK LMS-151	S+O	✓	✓	✓
2018	Complex Urban [248]	19	158.82	Outdoor	LiDAR	Velodyne VLP-16+SICK LMS-511	S+O	✓		✓
2018	In-House [12]	3		Outdoor	LiDAR	Velodyne HDL-64E		✓	✓	✓
2019	Semantic KITTI [249]	22	39.2	Outdoor	LiDAR	Velodyne HDL-64E	S+O	✓		✓
2019	Apollo-SouthBay [26]		>380	Outdoor	LiDAR	Velodyne HDL-64E		✓	✓	✓
2020	MulRan [250]	12	41.2	Outdoor	LiDAR+Radar	Ouster OS1-64	S+O	✓	✓	✓
2020	USyd [251]	>50		Outdoor	Camera+LiDAR	Velodyne VLP-16	S+O	✓	✓	✓
2020	Oxford Radar Robotcar [252]	>32	>280	Outdoor	Camera+LiDAR+Radar	Velodyne HDL-32E+SICK LMS-151+Navtech CTS350-X	S+O	✓	✓	✓
2021	DUT-AS [99]	30		Outdoor	LiDAR	SICK LMS 511	S+O	✓	✓	
2021	CMU Dataset [208]	11	2.0	Outdoor	Camera+LiDAR	Velodyne VLP-16		✓		
2021	Pittsburgh Dataset [208]	12	12.0	Outdoor	Camera+LiDAR	Velodyne VLP-16		✓		
2022	HAOMO [148]	5		Outdoor	Camera+LiDAR	HESAI PandarXT-32	S+O	✓	✓	✓
2022	Campus [55]	11	2	Outdoor	LiDAR	Velodyne-VLP 16		✓		
2022	City [55]	13	11	Outdoor	LiDAR	Velodyne-VLP 16		✓		
2022	KITTI-360 [253]	9	73.7	Outdoor	Camera+LiDAR	Velodyne HDL-64E	S+O	✓		✓
2022	CHDloop [94]	5	1.519	Outdoor	LiDAR	RoboSense RS-Ruby 128	S+O	✓		
2019	HKUST [79]			Indoor+Outdoor		Livox-MID40				✓
2022	LGSVL [146]			Outdoor		Velodyne HDL-64E		✓	✓	
2022	Real Vehicle [146]			Outdoor	Camera+LiDAR	Velodyne VLP-32C	S+O	✓		

where F_1 treated P and R as equally important. The maximum F_1 score (F_1^m) was then calculated as:

$$F_1^m = \max_{\tau} 2 \times \frac{P_{\tau} \times R_{\tau}}{P_{\tau} + R_{\tau}} \quad (7)$$

where the variable parameter τ could assume different roles, e.g., an algorithm parameter, a threshold representing the same place, or the number of retrieved candidates.

- Extended Precision (EP): It provided more comprehensive insights by simultaneously considering the lower and upper-performance bounds of an LPR method [71], [180], [196], [254]:

$$EP = \frac{1}{2} (P_{R0} + R_{P100}) \quad (8)$$

where P_{R0} was the precision at minimum recall, and R_{P100} was the max recall at 100% precision.

- Running Efficiency: Runtime was important to the online SLAM system. The time consumption of descriptor-based methods usually consisted of descriptor extraction and search. Map-based methods included map processing and matching while data-driven methods required training and inference.

10.3 Evaluation Results

To facilitate researchers in comprehending the performance of each method, we extensively gathered experimental evaluations on public datasets. As summarized in Table 4, we collected the publish year, method type, code, source of results, maximum F_1 score, EP [254], and runtime on KITTI Odometry [245]. Furthermore, Table 5 mainly summarized the publish year, code, source of results, AR, runtime, and

parameter size of learning-based methods on Oxford [247] and In-house [12] datasets.

11 CONCLUSIONS AND FUTURE DIRECTIONS

This paper is the first comprehensive survey specifically dedicated to LPR research to the best of our knowledge. It provides extensive discussions on the background of place recognition, highlighting the primary concerns in current research. We summarize commonly employed datasets and evaluation metrics. Furthermore, we conduct a comprehensive method classification and performance comparison, elucidating their architectures, strengths, and weaknesses. In this section, we also present promising trends for future evolution to promote and facilitate further research.

11.1 Learning-based Methods

Learning-based LPR methods have demonstrated impressive results, and we outline promising directions to improve their performance as follows:

- **Network Design.** Transformer-based networks [133], [143], [144], [147], [148] are computationally expensive for large-scale datasets. To address this, techniques like model compression and efficient attention mechanisms can be used to reduce computational requirements.
- **Loss Function.** The lazy quadruplet loss [12], [13], [143], [144], [150] is prone to overfitting with limited training data. Regularization techniques like weight decay, dropout, or batch normalization may enhance generalization performance.
- **Training Strategy.** End-to-end networks [9], [12], [13], [66], [129], [130], [140], [146], [152] commonly

Table 4: Evaluation results (Maximum F_1 , EP, and runtime) on KITTI Odometry [245] dataset. H and L represented handcrafted and learning-based methods, respectively. Source represented the source of results. EP referred to extended precision [254].

Year	Method	Type	Code	Source	Maximum F_1						EP						Time (ms)
					00	02	05	06	07	08	00	02	05	06	07	08	
2015	Fast Histogram [46]	H		[19], [148]	0.44	0.43				0.46							2
2016	M2DP [100]	H	✓	[71], [100]	0.71	0.72	0.60	0.79	0.56	0.07	0.62	0.60	0.61	0.68	0.59	0.50	366
2018	PointNetVLAD [12]	L	✓	[71]	0.78	0.73	0.54	0.85	0.63	0.04	0.64	0.69	0.54	0.77	0.59	0.50	
	SC [4]	H	✓	[71]	0.75	0.78	0.90	0.97	0.66	0.61	0.61	0.63	0.80	0.92	0.55	0.57	5
	SuMa [240]	H		[206], [240]		0.85											48
2019	SuMa++ [74]	L	✓	[74]							0.70	0.29					
	LPD-Net [5]	L		[119]		0.85											23
	ISC [44]	H	✓	[71]	0.66	0.71	0.77	0.84	0.64	0.41	0.63	0.61	0.73	0.82	0.64	0.54	4
2020	SGPR [49]	L	✓	[49], [71]	0.82	0.75	0.75	0.66	0.87	0.75	0.50	0.50	0.53	0.50	0.72	0.52	9
	OverlapNet [70], [206]	L	✓	[71], [148]	0.87	0.83	0.92	0.93	0.82	0.37	0.56	0.64	0.80	0.74	0.59	0.50	3238
	LocNet [19]	L		[19]	0.70	0.60				0.70							
	LocNet- Δr [19]	L		[19]	0.68	0.70				0.68							
2021	NDT-Transformer [144]	L	✓	[148]		0.85											16
	Minkloc3d [134]	L	✓	[148]		0.87											24
	Locus [180]	L	✓	[196], [198]	0.98	0.76	0.98	0.99	1.00	0.93	0.83		0.92	0.91	0.83	0.74	1210
	SSC-RN [71]	L	✓	[71]	0.94	0.89	0.94	0.99	0.87	0.88	0.83	0.75	0.90	0.97	0.77	0.73	5
	SSC-SK [71]	L	✓	[71]	0.95	0.89	0.95	0.99	0.88	0.94	0.85	0.75	0.90	0.97	0.81	0.93	5
	DiSCO [66]	L	✓	[198]	0.96	0.89	0.96	0.99	0.90	0.90							4310
	Gong <i>et al.</i> [186]	L		[186]	1.00	0.94	0.99	1.00	0.99	0.97							448
	LiDAR Iris [45]	H	✓	[45], [71]	0.67	0.76	0.77	0.91	0.63	0.48	0.63	0.67	0.75	0.79	0.65	0.56	231
	AttDLNet-E1 [149]	L	✓	[149]	0.90	0.82	0.86	0.98	0.11	0.73							3
	AttDLNet-E2 [149]	L	✓	[149]	0.93	0.78	0.86	1.00	0.11	0.73							4
	AttDLNet-E3 [149]	L	✓	[149]	0.92	0.78	0.87	1.00	0.11	0.74							10
	AttDLNet-E4 [149]	L	✓	[149]	0.94	0.79	0.82	0.98	0.11	0.73							19
	AttDLNet-E5 [149]	L	✓	[149]	0.94	0.55	0.85	0.95	0.13	0.68							24
	AttDLNet-E3A0 [149]	L	✓	[149]	0.92	0.77	0.87	1.00	0.11	0.73							10
	AttDLNet-E3A1 [149]	L	✓	[149]	0.95	0.82	0.88	1.00	0.11	0.75							13
	AttDLNet-E3A2 [149]	L	✓	[149]	0.94	0.74	0.87	0.99	0.11	0.72							16
	AttDLNet-E3A3 [149]	L	✓	[149]	0.94	0.80	0.88	0.99	0.10	0.74							19
	AttDLNet-E3A4 [149]	L	✓	[149]	0.94	0.82	0.90	1.00	0.10	0.75							20
	AttDLNet-E5A0 [149]	L	✓	[149]	0.94	0.55	0.85	0.95	0.13	0.68							24
	AttDLNet-E5A1 [149]	L	✓	[149]	0.91	0.62	0.77	0.99	0.11	0.68							13
	AttDLNet-E5A2 [149]	L	✓	[149]	0.94	0.54	0.89	0.98	0.09	0.69							16
	AttDLNet-E5A3 [149]	L	✓	[149]	0.94	0.79	0.85	0.98	0.10	0.73							19
	AttDLNet-E5A4 [149]	L	✓	[149]	0.95	0.69	0.86	0.99	0.10	0.72							20
2022	BG-RN [200]	L		[200]	0.99	0.97	0.96	1.00	1.00	0.79	0.99	0.93	0.95	0.99	1.00	0.79	
	BG-SK [200]	L		[200]	1.00	0.96	0.97	1.00	1.00	0.96	0.99	0.89	0.97	1.00	1.00	0.93	
	SC-LPR [209]	L	✓	[209]	0.97	0.95	0.93	0.99	0.99	0.88							224
	SC-LPR-K [209]	L	✓	[209]	0.93	0.93	0.93	0.99	0.99	0.83							224
	RINet-CY [198]	L	✓	[198]	0.98	0.95	0.92	0.98	0.97	0.87							211
	RINet-SK [198]	L	✓	[198]	0.99	0.95	0.95	1.00	1.00	0.96							211
	DSC [196]	L		[196]	0.88	0.84	0.78	0.86	0.82	0.85	0.70	0.68	0.63	0.73	0.58	0.65	50
	OverlapTransformer [148]	L	✓	[148]	0.88												2
	LOGG3D-Net [140]	L	✓	[140]	0.95	0.89	0.98	0.98	1.00	0.84							90
	CSSC [73]	H	✓	[73]	0.37		0.76			0.56							
2022	CSSC-TS [73]	H	✓	[73]	0.91		0.93			0.90							
	DeLightLCD [119]	L		[119]	0.90												2

demand large amounts of labeled data for training. Transfer learning and semi-supervised learning may enhance training efficiency.

11.2 Multi-modality Fusion

Integrating LiDAR with other sensors, such as IMU, cameras (monocular, stereo, depth), and radars, offers the opportunity to leverage complementary information and enhance the accuracy and robustness of place recognition. Exploring effective fusion strategies and developing algorithms that capitalize on the strengths of different sensor modalities represent a promising direction for future research.

11.3 Scalability and Efficiency

The growing affordability and accessibility of LiDAR sensors have spurred the demand for large-scale place recognition. This necessitates the development of scalable algorithms for handling large-scale point clouds and the design of efficient algorithms for the real-time processing of point cloud data on resource-constrained platforms.

11.4 Long-term Place Recognition

Long-term place recognition refers to the ability of a system to identify places over extended periods, despite appearance and weather variations. It is a crucial capability for autonomous navigation. Designing algorithms that can handle seasons, weathers, and appearances, and dynamic objects, will drive significant advancements in this field.

11.5 Datasets and Evaluation Metrics

Standardized datasets and evaluation metrics are crucial for fair comparisons in place recognition research. Creating diverse datasets that include various sensor modalities, environmental conditions, and weather variations while also defining additional performance evaluation metrics will advance the progress in this field.

REFERENCES

- [1] A. Torii, J. Sivic, M. Okutomi, and T. Pajdla, "Visual place recognition with repetitive structures," *IEEE Transactions on Pattern Analysis and Machine Intelligence*, vol. 37, no. 11, pp. 2346–2359, 2015.

Table 5: Evaluation results (AR @1 and @1%, runtime, and parameter size) of learning-based place recognition methods on Oxford RobotCar (Oxford) [247] and In-house datasets [12] including University Sector (U.S.), Residential Area (R.A.), and Business District (B.D.). AR referred to the average recall. Baseline represented that the network was trained using Oxford [247] dataset, while refine represented that the network was trained using Oxford [247] and in-house [12] datasets. Source represented the source of results. Para denoted the size of parameters.

Year	Method	Code	Source	Oxford		U.S.		R.A.		B.D.		Time (ms)	Para (Mb)		
				@1%	@1	@1%	@1	@1%	@1	@1%	@1				
2018	PointNetVLAD [12]	Baseline	✓	[12], [138]	80.3	62.8	72.6	63.2	60.3	56.1	65.3	57.2	15	19.8	
		Refine	✓	[12]	80.1	63.3	90.1	86.1	93.1	82.7	86.5	80.1			
	PointNetMax [12]	Baseline	✓	[12]	73.4		64.6		51.9		49.1				
		Refine	✓	[12]	73.9	54.2	79.3	62.2	75.14	60.21	69.5	58.6			
	PointNetSTD [12]	Baseline	✓	[12]	46.5		61.1		49.1		53.0				
		Refine	✓	[12]	46.5	31.9	57.0	45.7	59.8	44.3	53.0	44.5			
	PCAN [68]	Baseline	✓	[68], [134]	83.8	69.1	79.	62.4	71.2	57.0	66.8	58.1	55	20.4	
		Refine	✓	[68]	86.4	70.7	94.1	83.7	92.5	82.5	87.0	80.3			
2019	SeqLPD [226]			[226]	95.8	87.2							19	2.0	
		Baseline		[134], [138]	94.9	86.3	96.0	87.0	90.5	83.1	89.1	82.5	24	19.8	
	LPD-Net [5]	Baseline		[138]	94.9	86.6	98.9	94.4	96.4	90.8	94.4	90.8			
		Refine													
2020	DAGC [13]	Baseline		[13]	87.5		83.5		75.7		71.2				
		Refine		[13]	87.8	71.4	94.3	86.3	93.4	82.8	88.5	81.3			
	DH3D [69]	Baseline		[67], [69]	84.3	73.3	81.5	64.4	72.1	57.9	68.4	60.1	36	18.9	
		Refine													
	PIC-NET [150]	Baseline		[135]	98.2										
		Refine		[131]	94.6	86.8	94.3	86.8	89.2	80.2	83.5	77.3			
2021	SR-Net [131]	Baseline		[131]	95.3	88.5	98.5	93.5	93.6	86.8	90.8	85.9			
		Refine		[131]											
	PPT-Net [133]	Baseline	✓	[133]	98.1	93.5	97.5	90.1	93.3	84.1	90.0	84.6	22	13.1	
		Refine	✓	[133]	98.4		99.7		99.5		95.3				
	SOE-Net [129]	Baseline	✓	[67]	93.4	84.2	91.1	80.0	87.0	75.9	83.8	77.2	59	19.4	
		Refine	✓	[129]	96.4	89.3	97.7	91.8	95.9	90.2	92.6	89.0			
	MinkLoc3D [134]	Baseline	✓	[134]	98.5	94.8	99.7	97.2	99.3	96.7	96.7	94.0	21	1.1	
		Refine	✓	[134], [138]	98.5	94.8	99.7	97.2	99.3	96.7	96.7	94.0			
	Minkloc++ [135]	✓	[135]	99.1	96.7	99.5	96.5	98.5	95.3	95.5	91.8				
		NDT-Transformer [144]	✓	[139]	97.7	93.8								34	
	DiSCO [66]	✓	[66]	75.0	88.4									9	
		CORAL [18]	✓	[18]	96.1	88.9								11	
	vLPD-Net [132]	✓	[132]	73.14	53.45										
		TransLoc3D [137]	Baseline	[137]	98.5	95.0	94.9		91.5		88.4				
		Refine	[137]	98.5	95.0	99.8	97.5	99.7	97.3	97.4	94.8				
2022	SVT-Net [8]	Baseline		[8]	97.8	93.7	96.5	90.1	92.7	84.3	90.7	85.5	13	0.9	
		Refine		[8]	98.4	94.7	99.9	97.0	99.5	95.2	97.2	94.4	13	0.9	
	ASVT-Net [8]	Baseline		[8]	98.0	93.9	96.1	87.9	92.0	83.3	88.4	82.3	11	0.4	
		Refine		[8]	98.3	94.6	99.6	97.5	98.9	95.0	97.0	94.5	11	0.4	
	CSV-Net [8]	Baseline		[8]	97.7	93.1	95.5	88.3	92.3	82.7	89.5	83.3	12	0.8	
		Refine		[8]	98.6	94.8	99.8	96.6	98.7	96.2	97.3	94.3	12	0.8	
	EPC-Net [67]	✓	[67]	94.7	86.2	96.5	88.2	88.6	80.2	84.9	78.1	84.9	33	4.7	
		EPC-Net-L [67]	✓	[67]	86.5	73.0	82.9	68.9	76.9	62.5	72.2	64.0	26	0.4	
	EPC-Net-L-D [67]	✓	[67]	92.2	80.3	87.2	74.9	80.0	66.8	75.5	67.0	74.3	36	0.4	
		HiTPR [143]	✓	[143]	93.7	86.6	90.2	80.9	87.2	78.2	79.8	74.3	27		
	HiTPR-S8 [143]	✓	[143]	93.6	86.6	85.6	75.8	75.0	63.1	71.3	64.5	36	2.7		
		HiTPR-F8 [143]	✓	[143]	94.6	87.8	94.0	86.0	89.1	81.3	88.3	81.8			
	MinkLoc3D-I [139]	✓	[139]	98.1	93.6										
		MinkLoc3D-S [139]	✓	[139]	92.0	79.9									
	MinkLoc3D-SI [139]	✓	[139]	93.4	82.2									11	
		Retriever [14]	✓	[14]	91.9		91.9		87.4		85.5				
	MinkLoc3Dv2 [138]	Baseline	✓	[138]	98.9	96.3	96.7	90.9	93.8	86.5	91.2	86.3			
		Refine	✓	[138]	99.1	96.9	99.7	99.0	99.4	98.3	99.1	97.6			

[2] S. Lowry and M. J. Milford, "Supervised and unsupervised linear learning techniques for visual place recognition in changing environments," *IEEE Transactions on Robotics*, vol. 32, no. 3, pp. 600–613, 2016.

[3] D. L. Rizzini, "Place recognition of 3d landmarks based on geometric relations," in *2017 IEEE/RSJ International Conference on Intelligent Robots and Systems (IROS)*. IEEE, 2017, pp. 648–654.

[4] G. Kim and A. Kim, "Scan context: Egocentric spatial descriptor for place recognition within 3d point cloud map," in *2018 IEEE/RSJ International Conference on Intelligent Robots and Systems (IROS)*. IEEE, 2018, pp. 4802–4809.

[5] Z. Liu, S. Zhou, C. Suo, P. Yin, W. Chen, H. Wang, H. Li, and Y.-H. Liu, "Lpd-net: 3d point cloud learning for large-scale place recognition and environment analysis," in *Proceedings of the IEEE/CVF International Conference on Computer Vision*, 2019, pp. 2831–2840.

[6] P. Yin, F. Wang, A. Egorov, J. Hou, J. Zhang, and H. Choset, "Seqspherevlad: Sequence matching enhanced orientation-invariant place recognition," in *2020 IEEE/RSJ International Conference on Intelligent Robots and Systems (IROS)*, 2020, pp. 5024–5029.

[7] G. Kim, S. Choi, and A. Kim, "Scan context++: Structural place recognition robust to rotation and lateral variations in urban environments," *IEEE Transactions on Robotics*, 2021.

[8] Z. Fan, Z. Song, H. Liu, Z. Lu, J. He, and X. Du, "Svt-net: Super light-weight sparse voxel transformer for large scale place recognition," in *Proceedings of the AAAI Conference on Artificial Intelligence*, vol. 36, no. 1, 2022, pp. 551–560.

[9] G. Kim, B. Park, and A. Kim, "1-day learning, 1-year localization: Long-term lidar localization using scan context image," *IEEE Robotics and Automation Letters*, vol. 4, no. 2, pp. 1948–1955, 2019.

[10] H. Dong, X. Chen, and C. Stachniss, "Online range image-based pole extractor for long-term lidar localization in urban environments," in *2021 European Conference on Mobile Robots (ECMR)*. IEEE, 2021, pp. 1–6.

[11] F. Cao, H. Wu, and C. Wu, "An end-to-end localizer for long-term topological localization in large-scale changing environments," *IEEE Transactions on Industrial Electronics*, pp. 1–10, 2022.

[12] M. A. Uy and G. H. Lee, "Pointnetvlad: Deep point cloud based retrieval for large-scale place recognition," in *Proceedings of the IEEE conference on computer vision and pattern recognition*, 2018, pp. 4470–4479.

[13] Q. Sun, H. Liu, J. He, Z. Fan, and X. Du, "Dagc: Employing dual attention and graph convolution for point cloud based place recognition," in *Proceedings of the 2020 International Conference on Multimedia Retrieval*, 2020, pp. 224–232.

[14] L. Wiesmann, R. Marcuzzi, C. Stachniss, and J. Behley, "Retriever: Point cloud retrieval in compressed 3d maps," in *2022 International Conference on Robotics and Automation (ICRA)*, 2022, pp.

10 925–10 932.

[15] B. Steder, M. Ruhnke, S. Grzonka, and W. Burgard, “Place recognition in 3d scans using a combination of bag of words and point feature based relative pose estimation,” in *2011 IEEE/RSJ International Conference on Intelligent Robots and Systems*, 2011, pp. 1249–1255.

[16] A. Torii, R. Arandjelović, J. Sivic, M. Okutomi, and T. Pajdla, “24/7 place recognition by view synthesis,” *IEEE Transactions on Pattern Analysis and Machine Intelligence*, vol. 40, no. 2, pp. 257–271, 2018.

[17] A. Khalil, S. Ehsan, Z. Chen, M. Milford, and K. McDonald-Maier, “A holistic visual place recognition approach using lightweight cnns for significant viewpoint and appearance changes,” *IEEE transactions on robotics*, vol. 36, no. 2, pp. 561–569, 2019.

[18] Y. Pan, X. Xu, W. Li, Y. Cui, Y. Wang, and R. Xiong, “Coral: Colored structural representation for bi-modal place recognition,” in *2021 IEEE/RSJ International Conference on Intelligent Robots and Systems (IROS)*, 2021, pp. 2084–2091.

[19] H. Yin, Y. Wang, X. Ding, L. Tang, S. Huang, and R. Xiong, “3d lidar-based global localization using siamese neural network,” *IEEE Transactions on Intelligent Transportation Systems*, vol. 21, no. 4, pp. 1380–1392, 2020.

[20] S.-Y. An and J. Kim, “Extracting statistical signatures of geometry and structure in 2d occupancy grid maps for global localization,” *IEEE Robotics and Automation Letters*, vol. 7, no. 2, pp. 4291–4298, 2022.

[21] Y. Li, Y. Cai, Z. Li, S. Feng, H. Wang, and M. A. Sotelo, “Map-based localization for intelligent vehicles from bi-sensor data fusion,” *Expert Systems with Applications*, vol. 203, p. 117586, 2022.

[22] T. Schmiedel, E. Einhorn, and H.-M. Gross, “Iron: A fast interest point descriptor for robust ndt-map matching and its application to robot localization,” in *2015 IEEE/RSJ International Conference on Intelligent Robots and Systems (IROS)*. IEEE, 2015, pp. 3144–3151.

[23] H. Song, W. Choi, and H. Kim, “Robust vision-based relative-localization approach using an rgb-depth camera and lidar sensor fusion,” *IEEE Transactions on Industrial Electronics*, vol. 63, no. 6, pp. 3725–3736, 2016.

[24] A. Y. Hata and D. F. Wolf, “Feature detection for vehicle localization in urban environments using a multilayer lidar,” *IEEE Transactions on Intelligent Transportation Systems*, vol. 17, no. 2, pp. 420–429, 2016.

[25] G. Elbaz, T. Avraham, and A. Fischer, “3d point cloud registration for localization using a deep neural network auto-encoder,” in *Proceedings of the IEEE conference on computer vision and pattern recognition*, 2017, pp. 4631–4640.

[26] W. Lu, Y. Zhou, G. Wan, S. Hou, and S. Song, “L3-net: Towards learning based lidar localization for autonomous driving,” in *Proceedings of the IEEE/CVF Conference on Computer Vision and Pattern Recognition*, 2019, pp. 6389–6398.

[27] H. Wang, C. Wang, and L. Xie, “Lightweight 3-d localization and mapping for solid-state lidar,” *IEEE Robotics and Automation Letters*, vol. 6, no. 2, pp. 1801–1807, 2021.

[28] D. Schleicher, L. M. Bergasa, M. Ocaña, R. Barea, and M. E. López, “Real-time hierarchical outdoor slam based on stereovision and gps fusion,” *IEEE Transactions on Intelligent Transportation Systems*, vol. 10, no. 3, pp. 440–452, 2009.

[29] O. Vysotska, T. Naseer, L. Spinello, W. Burgard, and C. Stachniss, “Efficient and effective matching of image sequences under substantial appearance changes exploiting gps priors,” in *2015 IEEE International Conference on Robotics and Automation (ICRA)*, 2015, pp. 2774–2779.

[30] Y. Yang and G. Huang, “Observability analysis of aided ins with heterogeneous features of points, lines, and planes,” *IEEE Transactions on Robotics*, vol. 35, no. 6, pp. 1399–1418, 2019.

[31] K.-W. Chiang, G.-J. Tsai, H.-J. Chu, and N. El-Sheimy, “Performance enhancement of ins/gnss/refreshed-slam integration for acceptable lane-level navigation accuracy,” *IEEE Transactions on Vehicular Technology*, vol. 69, no. 3, pp. 2463–2476, 2020.

[32] J. J. Morales and Z. M. Kassas, “Tightly coupled inertial navigation system with signals of opportunity aiding,” *IEEE Transactions on Aerospace and Electronic Systems*, vol. 57, no. 3, pp. 1930–1948, 2021.

[33] G. P. C. Júnior, A. M. C. Rezende, V. R. F. Miranda, R. Fernandes, H. Azpúrua, A. A. Neto, G. Pessin, and G. M. Freitas, “Ekf-loam: An adaptive fusion of lidar slam with wheel odometry and inertial data for confined spaces with few geometric features,” *IEEE Transactions on Automation Science and Engineering*, vol. 19, no. 3, pp. 1458–1471, 2022.

[34] S. Lowry, N. Sünderhauf, P. Newman, J. J. Leonard, D. Cox, P. Corke, and M. J. Milford, “Visual place recognition: A survey,” *IEEE Transactions on Robotics*, vol. 32, no. 1, pp. 1–19, 2016.

[35] R. Power, M. Zaffar, B. Ferrarini, M. Milford, K. McDonald-Maier, and S. Ehsan, “A benchmark comparison of visual place recognition techniques for resource-constrained embedded platforms,” *arXiv preprint arXiv:2109.11002*, 2021.

[36] J. Peltomäki, F. Aljiani, J. Puura, H. Huttunen, E. Rahtu, and J.-K. Kämäräinen, “Evaluation of long-term lidar place recognition,” in *2021 IEEE/RSJ International Conference on Intelligent Robots and Systems (IROS)*, 2021, pp. 4487–4492.

[37] K. A. Tsintotas, L. Bampis, and A. Gasteratos, “The revisiting problem in simultaneous localization and mapping: A survey on visual loop closure detection,” *IEEE Transactions on Intelligent Transportation Systems*, vol. 23, no. 11, pp. 19 929–19 953, 2022.

[38] X. Zhang, L. Wang, and Y. Su, “Visual place recognition: A survey from deep learning perspective,” *Pattern Recognition*, vol. 113, p. 107760, 2021.

[39] J. Li, W. Xu, P. Shi, Y. Zhang, and Q. Hu, “Lnift: Locally normalized image for rotation invariant multimodal feature matching,” *IEEE Transactions on Geoscience and Remote Sensing*, vol. 60, pp. 1–14, 2022.

[40] J. Wu and J. M. Rehg, “Centrist: A visual descriptor for scene categorization,” *IEEE Transactions on Pattern Analysis and Machine Intelligence*, vol. 33, no. 8, pp. 1489–1501, 2011.

[41] R. Arandjelovic, P. Gronat, A. Torii, T. Pajdla, and J. Sivic, “Netvlad: Cnn architecture for weakly supervised place recognition,” in *Proceedings of the IEEE conference on computer vision and pattern recognition*, 2016, pp. 5297–5307.

[42] R. Wang, Y. Shen, W. Zuo, S. Zhou, and N. Zheng, “Transvpr: Transformer-based place recognition with multi-level attention aggregation,” in *Proceedings of the IEEE/CVF Conference on Computer Vision and Pattern Recognition*, 2022, pp. 13 648–13 657.

[43] P. Shi, Q. Ye, and L. Zeng, “A novel indoor structure extraction based on dense point cloud,” *ISPRS International Journal of Geoinformation*, vol. 9, no. 11, p. 660, 2020.

[44] H. Wang, C. Wang, and L. Xie, “Intensity scan context: Coding intensity and geometry relations for loop closure detection,” in *2020 IEEE International Conference on Robotics and Automation (ICRA)*. IEEE, 2020, pp. 2095–2101.

[45] Y. Wang, Z. Sun, C.-Z. Xu, S. E. Sarma, J. Yang, and H. Kong, “Lidar iris for loop-closure detection,” in *2020 IEEE/RSJ International Conference on Intelligent Robots and Systems (IROS)*. IEEE, 2020, pp. 5769–5775.

[46] T. Röhling, J. Mack, and D. Schulz, “A fast histogram-based similarity measure for detecting loop closures in 3-d lidar data,” in *2015 IEEE/RSJ International Conference on Intelligent Robots and Systems (IROS)*. IEEE, 2015, pp. 736–741.

[47] L. Luo, S.-Y. Cao, Z. Sheng, and H.-L. Shen, “Lidar-based global localization using histogram of orientations of principal normals,” *IEEE Transactions on Intelligent Vehicles*, vol. 7, no. 3, pp. 771–782, 2022.

[48] L. Schaupp, M. Bürki, R. Dubé, R. Siegwart, and C. Cadena, “Oreos: Oriented recognition of 3d point clouds in outdoor scenarios,” in *2019 IEEE/RSJ International Conference on Intelligent Robots and Systems (IROS)*. IEEE, 2019, pp. 3255–3261.

[49] X. Kong, X. Yang, G. Zhai, X. Zhao, X. Zeng, M. Wang, Y. Liu, W. Li, and F. Wen, “Semantic graph based place recognition for 3d point clouds,” in *2020 IEEE/RSJ International Conference on Intelligent Robots and Systems (IROS)*. IEEE, 2020, pp. 8216–8223.

[50] Y. Zhu, Y. Ma, L. Chen, C. Liu, M. Ye, and L. Li, “Gosmatch: Graph-of-semantics matching for detecting loop closures in 3d lidar data,” in *2020 IEEE/RSJ International Conference on Intelligent Robots and Systems (IROS)*. IEEE, 2020, pp. 5151–5157.

[51] L. Li, X. Kong, X. Zhao, W. Li, F. Wen, H. Zhang, and Y. Liu, “Saloom: Semantic-aided lidar slam with loop closure,” in *2021 IEEE International Conference on Robotics and Automation (ICRA)*. IEEE, 2021, pp. 7627–7634.

[52] L. Luo, S.-Y. Cao, B. Han, H.-L. Shen, and J. Li, “Bvmatch: Lidar-based place recognition using bird’s-eye view images,” *IEEE Robotics and Automation Letters*, vol. 6, no. 3, pp. 6076–6083, 2021.

[53] T. Shan, B. Englot, D. Meyers, W. Wang, C. Ratti, and D. Rus, “Lio-sam: Tightly-coupled lidar inertial odometry via smoothing and mapping,” in *2020 IEEE/RSJ International Conference on Intelligent Robots and Systems (IROS)*, 2020, pp. 5135–5142.

[54] Y. Zhang, "Lilo: A novel lidar-imu slam system with loop optimization," *IEEE Transactions on Aerospace and Electronic Systems*, 2021.

[55] P. Yin, F. Wang, A. Egorov, J. Hou, Z. Jia, and J. Han, "Fast sequence-matching enhanced viewpoint-invariant 3-d place recognition," *IEEE Transactions on Industrial Electronics*, vol. 69, no. 2, pp. 2127–2135, 2022.

[56] T. Shan and B. Englöt, "Lego-loam: Lightweight and ground-optimized lidar odometry and mapping on variable terrain," in *2018 IEEE/RSJ International Conference on Intelligent Robots and Systems (IROS)*. IEEE, 2018, pp. 4758–4765.

[57] P. Dellenbach, J.-E. Deschaud, B. Jacquet, and F. Goulette, "Cticp: Real-time elastic lidar odometry with loop closure," in *2022 International Conference on Robotics and Automation (ICRA)*, 2022, pp. 5580–5586.

[58] J. Li, P. Shi, Q. Hu, and Y. Zhang, "Qgore: Quadratic-time guaranteed outlier removal for point cloud registration," *IEEE Transactions on Pattern Analysis and Machine Intelligence*, 2023.

[59] M. Bosse and R. Zlot, "Place recognition using keypoint voting in large 3d lidar datasets," in *2013 IEEE International Conference on Robotics and Automation*, 2013, pp. 2677–2684.

[60] N. Muhammad and S. Lacroix, "Loop closure detection using small-sized signatures from 3d lidar data," in *2011 IEEE International Symposium on Safety, Security, and Rescue Robotics*. IEEE, 2011, pp. 333–338.

[61] J. Guo, P. V. Borges, C. Park, and A. Gawel, "Local descriptor for robust place recognition using lidar intensity," *IEEE Robotics and Automation Letters*, vol. 4, no. 2, pp. 1470–1477, 2019.

[62] K. P. Cop, P. V. Borges, and R. Dubé, "Delight: An efficient descriptor for global localisation using lidar intensities," in *2018 IEEE International Conference on Robotics and Automation (ICRA)*. IEEE, 2018, pp. 3653–3660.

[63] H. Xiang, W. Shi, W. Fan, P. Chen, S. Bao, and M. Nie, "Fastlcd: A fast and compact loop closure detection approach using 3d point cloud for indoor mobile mapping," *International Journal of Applied Earth Observation and Geoinformation*, vol. 102, p. 102430, 2021.

[64] S. Ratz, M. Dymczyk, R. Siegwart, and R. Dubé, "Oneshot global localization: Instant lidar-visual pose estimation," in *2020 IEEE International conference on Robotics and Automation (ICRA)*. IEEE, 2020, pp. 5415–5421.

[65] D. Xu, J. Liu, J. Hyppä, Y. Liang, and W. Tao, "A heterogeneous 3d map-based place recognition solution using virtual lidar and a polar grid height coding image descriptor," *ISPRS Journal of Photogrammetry and Remote Sensing*, vol. 183, pp. 1–18, 2022.

[66] X. Xu, H. Yin, Z. Chen, Y. Li, Y. Wang, and R. Xiong, "Disco: Differentiable scan context with orientation," *IEEE Robotics and Automation Letters*, vol. 6, no. 2, pp. 2791–2798, 2021.

[67] L. Hui, M. Cheng, J. Xie, J. Yang, and M.-M. Cheng, "Efficient 3d point cloud feature learning for large-scale place recognition," *IEEE Transactions on Image Processing*, vol. 31, pp. 1258–1270, 2022.

[68] W. Zhang and C. Xiao, "Pcan: 3d attention map learning using contextual information for point cloud based retrieval," in *Proceedings of the IEEE/CVF Conference on Computer Vision and Pattern Recognition*, 2019, pp. 12436–12445.

[69] J. Du, R. Wang, and D. Cremers, "Dh3d: Deep hierarchical 3d descriptors for robust large-scale 6dof relocation," in *European Conference on Computer Vision*. Springer, 2020, pp. 744–762.

[70] X. Chen, T. Lbe, A. Milioto, T. Rhling, and C. Stachniss, "Overlapnet: Loop closing for lidar-based slam," in *Robotics: Science and Systems 2020*, 2020.

[71] L. Li, X. Kong, X. Zhao, T. Huang, W. Li, F. Wen, H. Zhang, and Y. Liu, "Ssc: Semantic scan context for large-scale place recognition," in *2021 IEEE/RSJ International Conference on Intelligent Robots and Systems (IROS)*. IEEE, 2021, pp. 2092–2099.

[72] R. Dubé, D. Dugas, E. Stumm, J. Nieto, R. Siegwart, and C. Cadena, "Segmatch: Segment based place recognition in 3d point clouds," in *2017 IEEE International Conference on Robotics and Automation (ICRA)*, 2017, pp. 5266–5272.

[73] D. Xu, J. Liu, Y. Liang, X. Lv, and J. Hyppä, "A lidar-based single-shot global localization solution using a cross-section shape context descriptor," *ISPRS Journal of Photogrammetry and Remote Sensing*, vol. 189, pp. 272–288, 2022.

[74] X. Chen, A. Milioto, E. Palazzolo, P. Giguere, J. Behley, and C. Stachniss, "Suma++: Efficient lidar-based semantic slam," in *2019 IEEE/RSJ International Conference on Intelligent Robots and Systems (IROS)*. IEEE, 2019, pp. 4530–4537.

[75] X. Chen, I. Vizzo, T. Läbe, J. Behley, and C. Stachniss, "Range image-based lidar localization for autonomous vehicles," in *2021 IEEE International Conference on Robotics and Automation (ICRA)*, 2021, pp. 5802–5808.

[76] H. Wang, C. Wang, C.-L. Chen, and L. Xie, "F-loam : Fast lidar odometry and mapping," in *2021 IEEE/RSJ International Conference on Intelligent Robots and Systems (IROS)*, 2021, pp. 4390–4396.

[77] Y. Pan, P. Xiao, Y. He, Z. Shao, and Z. Li, "Mulls: Versatile lidar slam via multi-metric linear least square," in *2021 IEEE International Conference on Robotics and Automation (ICRA)*. IEEE, 2021, pp. 11633–11640.

[78] J. Zhang and S. Singh, "Low-drift and real-time lidar odometry and mapping," *Autonomous Robots*, vol. 41, no. 2, pp. 401–416, 2017.

[79] J. Lin and F. Zhang, "A fast, complete, point cloud based loop closure for lidar odometry and mapping," *arXiv preprint arXiv:1909.11811*, 2019.

[80] D. Wilson, X. Zhang, W. Sultani, and S. Wshah, "Visual and object geo-localization: A comprehensive survey," *arXiv preprint arXiv:2112.15202*, 2021.

[81] E. Mahdi and H. Xinning, "A survey on visual map localization using lidars and cameras," *arXiv preprint arXiv:2208.03376*, 2022.

[82] F. Chen, X. Wang, Y. Zhao, S. Lv, and X. Niu, "Visual object tracking: A survey," *Computer Vision and Image Understanding*, vol. 222, p. 103508, 2022.

[83] S. M. Marvasti-Zadeh, L. Cheng, H. Ghanei-Yakhdan, and S. Kasaei, "Deep learning for visual tracking: A comprehensive survey," *IEEE Transactions on Intelligent Transportation Systems*, 2021.

[84] I. A. Kazerouni, L. Fitzgerald, G. Dooley, and D. Toal, "A survey of state-of-the-art on visual slam," *Expert Systems with Applications*, p. 117734, 2022.

[85] S. Zhang, S. Zhao, D. An, J. Liu, H. Wang, Y. Feng, D. Li, and R. Zhao, "Visual slam for underwater vehicles: A survey," *Computer Science Review*, vol. 46, p. 100510, 2022.

[86] K. Huang, S. Zhang, J. Zhang, and D. Tao, "Event-based simultaneous localization and mapping: A comprehensive survey," *arXiv preprint arXiv:2304.09793*, 2023.

[87] C. Cadena, L. Carlone, H. Carrillo, Y. Latif, D. Scaramuzza, J. Neira, I. Reid, and J. J. Leonard, "Past, present, and future of simultaneous localization and mapping: Toward the robust-perception age," *IEEE Transactions on robotics*, vol. 32, no. 6, pp. 1309–1332, 2016.

[88] P. Yin, S. Zhao, I. Cisneros, A. Abuduweili, G. Huang, M. Milford, C. Liu, H. Choset, and S. Scherer, "General place recognition survey: Towards the real-world autonomy age," *arXiv preprint arXiv:2209.04497*, 2022.

[89] H. Yin, X. Xu, S. Lu, X. Chen, R. Xiong, S. Shen, C. Stachniss, and Y. Wang, "A survey on global lidar localization: Challenges, advances and open problems," *arXiv preprint arXiv:2302.07433*, 2023.

[90] X. Shi, Z. Chai, Y. Zhou, J. Wu, and Z. Xiong, "Global place recognition using an improved scan context for lidar-based localization system," in *2021 IEEE/ASME International Conference on Advanced Intelligent Mechatronics (AIM)*, 2021, pp. 498–503.

[91] X. Cai and W. Yin, "Weighted scan context: Global descriptor with sparse height feature for loop closure detection," in *2021 International Conference on Computer, Control and Robotics (ICCCR)*. IEEE, 2021, pp. 214–219.

[92] S. Lu, X. Xu, H. Yin, Z. Chen, R. Xiong, and Y. Wang, "One ring to rule them all: Radon sinogram for place recognition, orientation and translation estimation," in *2022 IEEE/RSJ International Conference on Intelligent Robots and Systems (IROS)*, 2022, pp. 2778–2785.

[93] X. Xu, S. Lu, J. Wu, H. Lu, Q. Zhu, Y. Liao, R. Xiong, and Y. Wang, "Ring++: Roto-translation invariant gram for global localization on a sparse scan map," *arXiv preprint arXiv:2210.05984*, 2022.

[94] W. Wang, H. Min, X. Wu, X. Hou, Y. Li, and X. Zhao, "High accuracy and low complexity lidar place recognition using unitary invariant frobenius norm," *IEEE Sensors Journal*, 2022.

[95] Y. Fan, X. Du, L. Luo, and J. Shen, "Fresco: Frequency-domain scan context for lidar-based place recognition with translation and rotation invariance," in *2022 17th International Conference on Control, Automation, Robotics and Vision (ICARCV)*. IEEE, 2022, pp. 576–583.

[96] F. Ou, Y. Li, and Z. Miao, "Place recognition of large-scale unstructured orchards with attention score maps," *IEEE Robotics and Automation Letters*, 2023.

[97] M. Magnusson, H. Andreasson, A. Nuchter, and A. J. Lilienthal, "Appearance-based loop detection from 3d laser data using the normal distributions transform," in *2009 IEEE International Conference on Robotics and Automation*. IEEE, 2009, pp. 23–28.

[98] J. Mo and J. Sattar, "A fast and robust place recognition approach for stereo visual odometry using lidar descriptors," in *2020 IEEE/RSJ International Conference on Intelligent Robots and Systems (IROS)*. IEEE, 2020, pp. 5893–5900.

[99] F. Cao, F. Yan, S. Wang, Y. Zhuang, and W. Wang, "Season-invariant and viewpoint-tolerant lidar place recognition in gps-denied environments," *IEEE Transactions on Industrial Electronics*, vol. 68, no. 1, pp. 563–574, 2021.

[100] L. He, X. Wang, and H. Zhang, "M2dp: A novel 3d point cloud descriptor and its application in loop closure detection," in *2016 IEEE/RSJ International Conference on Intelligent Robots and Systems (IROS)*. IEEE, 2016, pp. 231–237.

[101] L. Perdomo, D. Pittol, M. Mantelli, R. Maffei, M. Kolberg, and E. Prestes, "c-m2dp: A fast point cloud descriptor with color information to perform loop closure detection," in *2019 IEEE 15th International Conference on Automation Science and Engineering (CASE)*. IEEE, 2019, pp. 1145–1150.

[102] T. Cieslewski, E. Stumm, A. Gawel, M. Bosse, S. Lynam, and R. Siegwart, "Point cloud descriptors for place recognition using sparse visual information," in *2016 IEEE International Conference on Robotics and Automation (ICRA)*. IEEE, 2016, pp. 4830–4836.

[103] B. Steder, G. Grisetti, and W. Burgard, "Robust place recognition for 3d range data based on point features," in *2010 IEEE International Conference on Robotics and Automation*. IEEE, 2010, pp. 1400–1405.

[104] Y. Zhuang, N. Jiang, H. Hu, and F. Yan, "3-d-laser-based scene measurement and place recognition for mobile robots in dynamic indoor environments," *IEEE Transactions on Instrumentation and Measurement*, vol. 62, no. 2, pp. 438–450, 2013.

[105] F. Cao, Y. Zhuang, H. Zhang, and W. Wang, "Robust place recognition and loop closing in laser-based slam for ugv in urban environments," *IEEE Sensors Journal*, vol. 18, no. 10, pp. 4242–4252, 2018.

[106] T. Shan, B. Englot, F. Duarte, C. Ratti, and D. Rus, "Robust place recognition using an imaging lidar," in *2021 IEEE International Conference on Robotics and Automation (ICRA)*, 2021, pp. 5469–5475.

[107] B. Steder, G. Grisetti, M. Van Loock, and W. Burgard, "Robust on-line model-based object detection from range images," in *2009 IEEE/RSJ International Conference on Intelligent Robots and Systems*. IEEE, 2009, pp. 4739–4744.

[108] B. Steder, R. B. Rusu, K. Konolige, and W. Burgard, "Narf: 3d range image features for object recognition," in *Workshop on Defining and Solving Realistic Perception Problems in Personal Robotics at the IEEE/RSJ Int. Conf. on Intelligent Robots and Systems (IROS)*, vol. 44, 2010, p. 2.

[109] H. Bay, T. Tuytelaars, and L. Van Gool, "Surf: Speeded up robust features," in *European conference on computer vision*. Springer, 2006, pp. 404–417.

[110] E. Rublee, V. Rabaud, K. Konolige, and G. Bradski, "Orb: An efficient alternative to sift or surf," in *2011 International conference on computer vision*. Ieee, 2011, pp. 2564–2571.

[111] D. Gálvez-López and J. D. Tardos, "Bags of binary words for fast place recognition in image sequences," *IEEE Transactions on Robotics*, vol. 28, no. 5, pp. 1188–1197, 2012.

[112] J. Li, Q. Hu, and M. Ai, "Rift: Multi-modal image matching based on radiation-variation insensitive feature transform," *IEEE Transactions on Image Processing*, vol. 29, pp. 3296–3310, 2020.

[113] M. A. Fischler and R. C. Bolles, "Random sample consensus: a paradigm for model fitting with applications to image analysis and automated cartography," *Communications of the ACM*, vol. 24, no. 6, pp. 381–395, 1981.

[114] E. Rosten and T. Drummond, "Machine learning for high-speed corner detection," in *Computer Vision–ECCV 2006: 9th European Conference on Computer Vision, Graz, Austria, May 7–13, 2006. Proceedings, Part I 9*. Springer, 2006, pp. 430–443.

[115] H. Li, "Consensus set maximization with guaranteed global optimality for robust geometry estimation," in *2009 IEEE 12th International Conference on Computer Vision*. IEEE, 2009, pp. 1074–1080.

[116] M. Himstedt, J. Frost, S. Hellbach, H.-J. Böhme, and E. Maeble, "Large scale place recognition in 2d lidar scans using geometrical landmark relations," in *2014 IEEE/RSJ International Conference on Intelligent Robots and Systems*. IEEE, 2014, pp. 5030–5035.

[117] F. Kallasi and D. L. Rizzini, "Efficient loop closure based on falko lidar features for online robot localization and mapping," in *2016 IEEE/RSJ International Conference on Intelligent Robots and Systems (IROS)*. IEEE, 2016, pp. 1206–1213.

[118] F. Tombari, S. Salti, and L. D. Stefano, "Unique signatures of histograms for local surface description," in *European conference on computer vision*. Springer, 2010, pp. 356–369.

[119] H. Xiang, X. Zhu, W. Shi, W. Fan, P. Chen, and S. Bao, "Delightlcd: A deep and lightweight network for loop closure detection in lidar slam," *IEEE Sensors Journal*, vol. 22, no. 21, pp. 20761–20772, 2022.

[120] Y. Zhou, Y. Wang, F. Poiesi, Q. Qin, and Y. Wan, "Loop closure detection using local 3d deep descriptors," *IEEE Robotics and Automation Letters*, vol. 7, no. 3, pp. 6335–6342, 2022.

[121] F. Poiesi and D. Boscaini, "Distinctive 3d local deep descriptors," in *2020 25th International conference on pattern recognition (ICPR)*. IEEE, 2021, pp. 5720–5727.

[122] Y. Zhong, "Intrinsic shape signatures: A shape descriptor for 3d object recognition," in *2009 IEEE 12th international conference on computer vision workshops, ICCV Workshops*. IEEE, 2009, pp. 689–696.

[123] M. Frosi and M. Matteucci, "Art-slam: Accurate real-time 6dof lidar slam," *IEEE Robotics and Automation Letters*, vol. 7, no. 2, pp. 2692–2699, 2022.

[124] L. Liao, C. Fu, B. Feng, and T. Su, "Optimized sc-f-loam: Optimized fast lidar odometry and mapping using scan context," in *2022 6th CAA International Conference on Vehicular Control and Intelligence (CVCI)*, 2022, pp. 1–6.

[125] W. Chen, Y. Wang, H. Chen, and Y. Liu, "Eil-slam: Depth-enhanced edge-based infrared-lidar slam," *Journal of Field Robotics*, vol. 39, no. 2, pp. 117–130, 2022.

[126] M. Magnusson, T. P. Kucner, S. G. Shahbandi, H. Andreasson, and A. J. Lilienthal, "Semi-supervised 3d place categorisation by descriptor clustering," in *2017 IEEE/RSJ International Conference on Intelligent Robots and Systems (IROS)*. IEEE, 2017, pp. 620–625.

[127] D. Arthur and S. Vassilvitskii, "k-means++: The advantages of careful seeding," Stanford, Tech. Rep., 2006.

[128] Q. Meng, H. Guo, X. Zhao, D. Cao, and H. Chen, "Loop-closure detection with a multiresolution point cloud histogram mode in lidar odometry and mapping for intelligent vehicles," *IEEE/ASME Transactions on Mechatronics*, vol. 26, no. 3, pp. 1307–1317, 2021.

[129] Y. Xia, Y. Xu, S. Li, R. Wang, J. Du, D. Cremers, and U. Still, "Soenet: A self-attention and orientation encoding network for point cloud based place recognition," in *2021 IEEE/CVF Conference on Computer Vision and Pattern Recognition (CVPR)*. IEEE, 2021, pp. 11343–11352.

[130] D. Cattaneo, M. Vaghi, and A. Valada, "Lcdnet: Deep loop closure detection and point cloud registration for lidar slam," *IEEE Transactions on Robotics*, vol. 38, no. 4, pp. 2074–2093, 2022.

[131] Z. Fan, H. Liu, J. He, Q. Sun, and X. Du, "Srnet: A 3d scene recognition network using static graph and dense semantic fusion," in *Computer Graphics Forum*, vol. 39, no. 7. Wiley Online Library, 2020, pp. 301–311.

[132] Z. Qiao, H. Hu, W. Shi, S. Chen, Z. Liu, and H. Wang, "A registration-aided domain adaptation network for 3d point cloud based place recognition," in *2021 IEEE/RSJ International Conference on Intelligent Robots and Systems (IROS)*. IEEE, 2021, pp. 1317–1322.

[133] L. Hui, H. Yang, M. Cheng, J. Xie, and J. Yang, "Pyramid point cloud transformer for large-scale place recognition," in *Proceedings of the IEEE/CVF International Conference on Computer Vision*, 2021, pp. 6098–6107.

[134] J. Komorowski, "Minkloc3d: Point cloud based large-scale place recognition," in *Proceedings of the IEEE/CVF Winter Conference on Applications of Computer Vision*, 2021, pp. 1790–1799.

[135] J. Komorowski, M. Wysoczańska, and T. Trzcinski, "Minkloc++: Lidar and monocular image fusion for place recognition," in *2021 International Joint Conference on Neural Networks (IJCNN)*, 2021, pp. 1–8.

[136] J. Komorowski, M. Wysoczańska, and T. Trzcinski, "Egonn: Ego-centric neural network for point cloud based 6dof relocalization

at the city scale," *IEEE Robotics and Automation Letters*, vol. 7, no. 2, pp. 722–729, 2021.

[137] T.-X. Xu, Y.-C. Guo, Y.-K. Lai, and S.-H. Zhang, "Transloc3d: Point cloud based large-scale place recognition using adaptive receptive fields," *arXiv preprint arXiv:2105.11605*, 2021.

[138] J. Komorowski, "Improving point cloud based place recognition with ranking-based loss and large batch training," in *2022 26th International Conference on Pattern Recognition (ICPR)*. IEEE, 2022, pp. 3699–3705.

[139] K. Źywanowski, A. Banaszczyk, M. R. Nowicki, and J. Komorowski, "Minkloc3d-si: 3d lidar place recognition with sparse convolutions, spherical coordinates, and intensity," *IEEE Robotics and Automation Letters*, vol. 7, no. 2, pp. 1079–1086, 2022.

[140] K. Vidanapathirana, M. Ramezani, P. Moghadam, S. Sridharan, and C. Fookes, "Log3d-net: Locally guided global descriptor learning for 3d place recognition," in *2022 International Conference on Robotics and Automation (ICRA)*. IEEE, 2022, pp. 2215–2221.

[141] M. Y. Chang, S. Yeon, S. Ryu, and D. Lee, "Spoxelnet: Spherical voxel-based deep place recognition for 3d point clouds of crowded indoor spaces," in *2020 IEEE/RSJ International Conference on Intelligent Robots and Systems (IROS)*. IEEE, 2020, pp. 8564–8570.

[142] S. Siva, Z. Nahman, and H. Zhang, "Voxel-based representation learning for place recognition based on 3d point clouds," in *2020 IEEE/RSJ International Conference on Intelligent Robots and Systems (IROS)*, 2020, pp. 8351–8357.

[143] Z. Hou, Y. Yan, C. Xu, and H. Kong, "Hitpr: Hierarchical transformer for place recognition in point cloud," in *2022 International Conference on Robotics and Automation (ICRA)*. IEEE, 2022, pp. 2612–2618.

[144] Z. Zhou, C. Zhao, D. Adolfsson, S. Su, Y. Gao, T. Duckett, and L. Sun, "Ndt-transformer: Large-scale 3d point cloud localisation using the normal distribution transform representation," in *2021 IEEE International Conference on Robotics and Automation (ICRA)*. IEEE, 2021, pp. 5654–5660.

[145] H. Yin, X. Ding, L. Tang, Y. Wang, and R. Xiong, "Efficient 3d lidar based loop closing using deep neural network," in *2017 IEEE International Conference on Robotics and Biomimetics (ROBIO)*. IEEE, 2017, pp. 481–486.

[146] D. Kong, X. Li, Y. Cen, Q. Xu, and A. Wang, "Simultaneous viewpoint- and condition-invariant loop closure detection based on lidar descriptor for outdoor large-scale environments," *IEEE Transactions on Industrial Electronics*, vol. 70, no. 2, pp. 2117–2127, 2023.

[147] J. Ma, X. Chen, J. Xu, and G. Xiong, "Seqot: A spatial-temporal transformer network for place recognition using sequential lidar data," *IEEE Transactions on Industrial Electronics*, 2022.

[148] J. Ma, J. Zhang, J. Xu, R. Ai, W. Gu, and X. Chen, "Overlap-transformer: An efficient and yaw-angle-invariant transformer network for lidar-based place recognition," *IEEE Robotics and Automation Letters*, vol. 7, no. 3, pp. 6958–6965, 2022.

[149] T. Barros, L. Garrote, R. Pereira, C. Premeida, and U. J. Nunes, "Attdlnet: Attention-based dl network for 3d lidar place recognition," *arXiv preprint arXiv:2106.09637*, 2021.

[150] Y. Lu, F. Yang, F. Chen, and D. Xie, "Pic-net: Point cloud and image collaboration network for large-scale place recognition," *arXiv preprint arXiv:2008.00658*, 2020.

[151] L. Bernreiter, L. Ott, J. Nieto, R. Siegwart, and C. Cadena, "Spherical multi-modal place recognition for heterogeneous sensor systems," in *2021 IEEE International Conference on Robotics and Automation (ICRA)*. IEEE, 2021, pp. 1743–1750.

[152] H. Lai, P. Yin, and S. Scherer, "Adafusion: Visual-lidar fusion with adaptive weights for place recognition," *IEEE Robotics and Automation Letters*, vol. 7, no. 4, pp. 12 038–12 045, 2022.

[153] C. R. Qi, H. Su, K. Mo, and L. J. Guibas, "Pointnet: Deep learning on point sets for 3d classification and segmentation," in *Proceedings of the IEEE conference on computer vision and pattern recognition*, 2017, pp. 652–660.

[154] S. Chopra, R. Hadsell, and Y. LeCun, "Learning a similarity metric discriminatively, with application to face verification," in *2005 IEEE Computer Society Conference on Computer Vision and Pattern Recognition (CVPR'05)*, vol. 1. IEEE, 2005, pp. 539–546.

[155] S. Shi, C. Guo, L. Jiang, Z. Wang, J. Shi, X. Wang, and H. Li, "Pv-rcnn: Point-voxel feature set abstraction for 3d object detection," in *Proceedings of the IEEE/CVF Conference on Computer Vision and Pattern Recognition*, 2020, pp. 10 529–10 538.

[156] F. Groh, P. Wieschollek, and H. P. Lensch, "Flex-convolution: Million-scale point-cloud learning beyond grid-worlds," in *Computer Vision–ACCV 2018: 14th Asian Conference on Computer Vision, Perth, Australia, December 2–6, 2018, Revised Selected Papers, Part I* 14. Springer, 2019, pp. 105–122.

[157] J. Hu, L. Shen, and G. Sun, "Squeeze-and-excitation networks," in *Proceedings of the IEEE conference on computer vision and pattern recognition*, 2018, pp. 7132–7141.

[158] H. Deng, T. Birdal, and S. Ilic, "Ppfnet: Global context aware local features for robust 3d point matching," in *2018 IEEE/CVF Conference on Computer Vision and Pattern Recognition*, 2018, pp. 195–205.

[159] Y. Wang, Y. Sun, Z. Liu, S. E. Sarma, M. M. Bronstein, and J. M. Solomon, "Dynamic graph cnn for learning on point clouds," *Acm Transactions On Graphics (tog)*, vol. 38, no. 5, pp. 1–12, 2019.

[160] C. R. Qi, L. Yi, H. Su, and L. J. Guibas, "Pointnet++: Deep hierarchical feature learning on point sets in a metric space," *Advances in neural information processing systems*, vol. 30, 2017.

[161] T.-Y. Lin, P. Dollár, R. Girshick, K. He, B. Hariharan, and S. Belongie, "Feature pyramid networks for object detection," in *Proceedings of the IEEE conference on computer vision and pattern recognition*, 2017, pp. 2117–2125.

[162] ———, "Feature pyramid networks for object detection," in *Proceedings of the IEEE conference on computer vision and pattern recognition*, 2017, pp. 2117–2125.

[163] Q. Wang, B. Wu, P. Zhu, P. Li, W. Zuo, and Q. Hu, "Eca-net: Efficient channel attention for deep convolutional neural networks," in *2020 IEEE/CVF Conference on Computer Vision and Pattern Recognition (CVPR)*, 2020, pp. 11 531–11 539.

[164] K. He, X. Zhang, S. Ren, and J. Sun, "Deep residual learning for image recognition," in *2016 IEEE Conference on Computer Vision and Pattern Recognition (CVPR)*, 2016, pp. 770–778.

[165] A. Brown, W. Xie, V. Kalogeiton, and A. Zisserman, "Smooth-ap: Smoothing the path towards large-scale image retrieval," in *Computer Vision–ECCV 2020: 16th European Conference, Glasgow, UK, August 23–28, 2020, Proceedings, Part IX 16*. Springer, 2020, pp. 677–694.

[166] J. Revaud, J. Almazán, R. S. Rezende, and C. R. d. Souza, "Learning with average precision: Training image retrieval with a listwise loss," in *Proceedings of the IEEE/CVF International Conference on Computer Vision*, 2019, pp. 5107–5116.

[167] A. Vaswani, N. Shazeer, N. Parmar, J. Uszkoreit, L. Jones, A. N. Gomez, Ł. Kaiser, and I. Polosukhin, "Attention is all you need," *Advances in neural information processing systems*, vol. 30, 2017.

[168] C. Choy, J. Gwak, and S. Savarese, "4d spatio-temporal convnets: Minkowski convolutional neural networks," in *Proceedings of the IEEE/CVF conference on computer vision and pattern recognition*, 2019, pp. 3075–3084.

[169] H. Tang, Z. Liu, S. Zhao, Y. Lin, J. Lin, H. Wang, and S. Han, "Searching efficient 3d architectures with sparse point-voxel convolution," in *Computer Vision–ECCV 2020: 16th European Conference, Glasgow, UK, August 23–28, 2020, Proceedings, Part XXVIII*. Springer, 2020, pp. 685–702.

[170] T.-L. Habich, M. Stuedle, M. Labb  , and S. Spindeldreier, "Have i been here before? learning to close the loop with lidar data in graph-based slam," in *2021 IEEE/ASME International Conference on Advanced Intelligent Mechatronics (AIM)*. IEEE, 2021, pp. 504–510.

[171] K. Granstr  m and T. B. Sch  n, "Learning to close the loop from 3d point clouds," in *2010 IEEE/RSJ International Conference on Intelligent Robots and Systems*, 2010, pp. 2089–2095.

[172] Y. Freund and R. E. Schapire, "A decision-theoretic generalization of on-line learning and an application to boosting," *Journal of computer and system sciences*, vol. 55, no. 1, pp. 119–139, 1997.

[173] F. Radenovi  , G. Tolias, and O. Chum, "Fine-tuning cnn image retrieval with no human annotation," *IEEE Transactions on Pattern Analysis and Machine Intelligence*, vol. 41, no. 7, pp. 1655–1668, 2019.

[174] J.-Y. Zhu, T. Park, P. Isola, and A. A. Efros, "Unpaired image-to-image translation using cycle-consistent adversarial networks," in *Proceedings of the IEEE international conference on computer vision*, 2017, pp. 2223–2232.

[175] T. S. Cohen, M. Geiger, J. K  hler, and M. Welling, "Spherical cnns," *arXiv preprint arXiv:1801.10130*, 2018.

[176] C. Esteves, C. Allen-Blanchette, A. Makadia, and K. Daniilidis, "Learning so (3) equivariant representations with spherical

cnns," in *Proceedings of the European Conference on Computer Vision (ECCV)*, 2018, pp. 52–68.

[177] N. Perraudin, M. Defferrard, T. Kacprzak, and R. Sgier, "Deep-sphere: Efficient spherical convolutional neural network with healpix sampling for cosmological applications," *Astronomy and Computing*, vol. 27, pp. 130–146, 2019.

[178] P. Besl and N. D. McKay, "A method for registration of 3-d shapes," *IEEE Transactions on Pattern Analysis and Machine Intelligence*, vol. 14, no. 2, pp. 239–256, 1992.

[179] R. Dube, A. Cramariuc, D. Dugas, J. Nieto, R. Siegwart, and C. Cadena, "Segmap: 3d segment mapping using data-driven descriptors," in *Robotics: Science and Systems*, 2018.

[180] K. Vidanapathirana, P. Moghadam, B. Harwood, M. Zhao, S. Sridharan, and C. Fookes, "Locus: Lidar-based place recognition using spatiotemporal higher-order pooling," in *2021 IEEE International Conference on Robotics and Automation (ICRA)*. IEEE, 2021, pp. 5075–5081.

[181] R. Dubé, M. G. Gollub, H. Sommer, I. Gilitschenski, R. Siegwart, C. Cadena, and J. Nieto, "Incremental-segment-based localization in 3-d point clouds," *IEEE Robotics and Automation Letters*, vol. 3, no. 3, pp. 1832–1839, 2018.

[182] X. Ji, L. Zuo, C. Zhang, and Y. Liu, "Lloam: Lidar odometry and mapping with loop-closure detection based correction," in *2019 IEEE International Conference on Mechatronics and Automation (ICMA)*. IEEE, 2019, pp. 2475–2480.

[183] R. Dubé, A. Gawel, H. Sommer, J. Nieto, R. Siegwart, and C. Cadena, "An online multi-robot slam system for 3d lidars," in *2017 IEEE/RSJ International Conference on Intelligent Robots and Systems (IROS)*, 2017, pp. 1004–1011.

[184] J. Li, J. Zhao, Y. Kang, X. He, C. Ye, and L. Sun, "Dl-slam: Direct 2.5d lidar slam for autonomous driving," in *2019 IEEE Intelligent Vehicles Symposium (IV)*, 2019, pp. 1205–1210.

[185] Y. Xie, Y. Zhang, L. Chen, H. Cheng, W. Tu, D. Cao, and Q. Li, "Rdc-slam: A real-time distributed cooperative slam system based on 3d lidar," *IEEE Transactions on Intelligent Transportation Systems*, 2021.

[186] Y. Gong, F. Sun, J. Yuan, W. Zhu, and Q. Sun, "A two-level framework for place recognition with 3d lidar based on spatial relation graph," *Pattern Recognition*, vol. 120, p. 108171, 2021.

[187] Y. Fan, Y. He, and U.-X. Tan, "Seed: A segmentation-based egocentric 3d point cloud descriptor for loop closure detection," in *2020 IEEE/RSJ International Conference on Intelligent Robots and Systems (IROS)*. IEEE, 2020, pp. 5158–5163.

[188] G. Tinchev, A. Penate-Sánchez, and M. Fallon, "Learning to see the wood for the trees: Deep laser localization in urban and natural environments on a cpu," *IEEE Robotics and Automation Letters*, vol. 4, no. 2, pp. 1327–1334, 2019.

[189] Y. Li, R. Bu, M. Sun, W. Wu, X. Di, and B. Chen, "Pointcnn: Convolution on x-transformed points," in *NeurIPS*, 2018.

[190] G. Tinchev, S. Nobili, and M. Fallon, "Seeing the wood for the trees: Reliable localization in urban and natural environments," in *2018 IEEE/RSJ International Conference on Intelligent Robots and Systems (IROS)*, 2018, pp. 8239–8246.

[191] R. Dube, A. Cramariuc, D. Dugas, H. Sommer, M. Dymczyk, J. Nieto, R. Siegwart, and C. Cadena, "Segmap: Segment-based mapping and localization using data-driven descriptors," *The International Journal of Robotics Research*, vol. 39, no. 2–3, pp. 339–355, 2020.

[192] D. Rozenberszki and A. L. Majdik, "Lol: Lidar-only odometry and localization in 3d point cloud maps," in *2020 IEEE International Conference on Robotics and Automation (ICRA)*, 2020, pp. 4379–4385.

[193] A. Cramariuc, F. Tschopp, N. Alatur, S. Benz, T. Falck, M. Brühlmeier, B. Hahn, J. Nieto, and R. Siegwart, "Semsegmap–3d segment-based semantic localization," in *2021 IEEE/RSJ International Conference on Intelligent Robots and Systems (IROS)*. IEEE, 2021, pp. 1183–1190.

[194] J. Wietrzykowski and P. Skrzypczyński, "On the descriptive power of lidar intensity images for segment-based loop closing in 3-d slam," in *2021 IEEE/RSJ International Conference on Intelligent Robots and Systems (IROS)*, 2021, pp. 79–85.

[195] I. Bogoslavskyi and C. Stachniss, "Fast range image-based segmentation of sparse 3d laser scans for online operation," in *2016 IEEE/RSJ International Conference on Intelligent Robots and Systems (IROS)*, 2016, pp. 163–169.

[196] J. Cui, Y. Cai, T. Huang, J. Zhao, L. Xiong, and Z. Yu, "Dsc: Deep scan context descriptor for large-scale place recognition," in *2022 IEEE International Conference on Multisensor Fusion and Integration for Intelligent Systems (MFIS)*. IEEE, 2022, pp. 1–7.

[197] A. Milioto, I. Vizzo, J. Behley, and C. Stachniss, "Rangenet++: Fast and accurate lidar semantic segmentation," in *2019 IEEE/RSJ international conference on intelligent robots and systems (IROS)*. IEEE, 2019, pp. 4213–4220.

[198] L. Li, X. Kong, X. Zhao, T. Huang, W. Li, F. Wen, H. Zhang, and Y. Liu, "Rinet: Efficient 3d lidar-based place recognition using rotation invariant neural network," *IEEE Robotics and Automation Letters*, vol. 7, no. 2, pp. 4321–4328, 2022.

[199] A. Gawel, C. Del Don, R. Siegwart, J. Nieto, and C. Cadena, "X-view: Graph-based semantic multi-view localization," *IEEE Robotics and Automation Letters*, vol. 3, no. 3, pp. 1687–1694, 2018.

[200] G. Pramatarov, D. De Martini, M. Gadd, and P. Newman, "Boxgraph: Semantic place recognition and pose estimation from 3d lidar," *arXiv preprint arXiv:2206.15154*, 2022.

[201] L. Li, X. Kong, X. Zhao, T. Huang, and Y. Liu, "Semantic scan context: a novel semantic-based loop-closure method for lidar slam," *Autonomous Robots*, vol. 46, no. 4, pp. 535–551, 2022.

[202] H. Yuan, Y. Zhang, S. Fan, X. Li, and J. Wang, "Object scan context: Object-centric spatial descriptor for place recognition within 3d point cloud map," *arXiv preprint arXiv:2206.03062*, 2022.

[203] A. Zaganidis, A. Zerntev, T. Duckett, and G. Cielniak, "Semantically assisted loop closure in slam using ndt histograms," in *2019 IEEE/RSJ International Conference on Intelligent Robots and Systems (IROS)*. IEEE, 2019, pp. 4562–4568.

[204] M. Magnusson, H. Andreasson, A. Nuchter, and A. J. Lilienthal, "Automatic appearance-based loop detection from three-dimensional laser data using the normal distributions transform," *Journal of Field Robotics*, vol. 26, no. 11–12, pp. 892–914, 2009.

[205] L. Bernreiter, A. Gawel, H. Sommer, J. Nieto, R. Siegwart, and C. C. Lerma, "Multiple hypothesis semantic mapping for robust data association," *IEEE Robotics and Automation Letters*, vol. 4, no. 4, pp. 3255–3262, 2019.

[206] X. Chen, T. Läbe, A. Milioto, T. Röhling, J. Behley, and C. Stachniss, "Overlapnet: a siamese network for computing lidar scan similarity with applications to loop closing and localization," *Autonomous Robots*, vol. 46, no. 1, pp. 61–81, 2022.

[207] X. Chen, T. Läbe, L. Nardi, J. Behley, and C. Stachniss, "Learning an overlap-based observation model for 3d lidar localization," in *2020 IEEE/RSJ International Conference on Intelligent Robots and Systems (IROS)*, 2020, pp. 4602–4608.

[208] P. Yin, L. Xu, Z. Feng, A. Egorov, and B. Li, "Pse-match: A viewpoint-free place recognition method with parallel semantic embedding," *IEEE Transactions on Intelligent Transportation Systems*, 2021.

[209] D. Dai, J. Wang, Z. Chen, and P. Bao, "Sc-lpr: Spatiotemporal context based lidar place recognition," *Pattern Recognition Letters*, vol. 156, pp. 160–166, 2022.

[210] Y. Bai, H. Ding, S. Bian, T. Chen, Y. Sun, and W. Wang, "Simgnn: A neural network approach to fast graph similarity computation," in *Proceedings of the twelfth ACM international conference on web search and data mining*, 2019, pp. 384–392.

[211] K. Ebadi, Y. Chang, M. Palieri, A. Stephens, A. Hatteland, E. Heiden, A. Thakur, N. Funabiki, B. Morrell, S. Wood, L. Carbone, and A.-a. Agha-mohammadi, "Lamp: Large-scale autonomous mapping and positioning for exploration of perceptually-degraded subterranean environments," in *2020 IEEE International Conference on Robotics and Automation (ICRA)*, 2020, pp. 80–86.

[212] N. Rottmann, R. Bruder, A. Schweikard, and E. Rueckert, "Loop closure detection in closed environments," in *2019 European Conference on Mobile Robots (ECMR)*. IEEE, 2019, pp. 1–8.

[213] C. Wen, Y. Dai, Y. Xia, Y. Lian, J. Tan, C. Wang, and J. Li, "Toward efficient 3-d colored mapping in gps-/gnss-denied environments," *IEEE Geoscience and Remote Sensing Letters*, vol. 17, no. 1, pp. 147–151, 2020.

[214] B. Zhou, Y. He, K. Qian, X. Ma, and X. Li, "S4-slam: A real-time 3d lidar slam system for ground/watersurface multi-scene outdoor applications," *Autonomous Robots*, vol. 45, no. 1, pp. 77–98, 2021.

[215] E. Mendes, P. Koch, and S. Lacroix, "Icp-based pose-graph slam," in *2016 IEEE International Symposium on Safety, Security, and Rescue Robotics (SSRR)*. IEEE, 2016, pp. 195–200.

[216] C. Le Gentil, T. Vidal-Calleja, and S. Huang, "In2lama: Inertial lidar localization autocalibration and mapping," *IEEE Transactions on Robotics*, vol. 37, no. 1, pp. 275–290, 2020.

[217] J. Jiang, J. Wang, P. Wang, P. Bao, and Z. Chen, "Lipmatch: Lidar point cloud plane based loop-closure," *IEEE Robotics and Automation Letters*, vol. 5, no. 4, pp. 6861–6868, 2020.

[218] M. Yokozuka, K. Koide, S. Oishi, and A. Banno, "Litamin: Lidar-based tracking and mapping by stabilized icp for geometry approximation with normal distributions," in *2020 IEEE/RSJ International Conference on Intelligent Robots and Systems (IROS)*, 2020, pp. 5143–5150.

[219] —, "Litamin2: Ultra light lidar-based slam using geometric approximation applied with kl-divergence," in *2021 IEEE International Conference on Robotics and Automation (ICRA)*. IEEE, 2021, pp. 11619–11625.

[220] A. Segal, D. Haehnel, and S. Thrun, "Generalized-icp," in *Robotics: science and systems*, vol. 2, no. 4. Seattle, WA, 2009, p. 435.

[221] J. G. Mangelson, D. Dominic, R. M. Eustice, and R. Vasudevan, "Pairwise consistent measurement set maximization for robust multi-robot map merging," in *2018 IEEE International Conference on Robotics and Automation (ICRA)*, 2018, pp. 2916–2923.

[222] Y. Chang, K. Ebadi, C. E. Denniston, M. F. Ginting, A. Rosinol, A. Reinke, M. Palieri, J. Shi, A. Chatterjee, B. Morrell, A.-a. Agha-mohammadi, and L. Carlone, "Lamp 2.0: A robust multi-robot slam system for operation in challenging large-scale underground environments," *IEEE Robotics and Automation Letters*, vol. 7, no. 4, pp. 9175–9182, 2022.

[223] H. Yang, J. Shi, and L. Carlone, "Teaser: Fast and certifiable point cloud registration," *IEEE Transactions on Robotics*, vol. 37, no. 2, pp. 314–333, 2021.

[224] Z. Gong, J. Li, Z. Luo, C. Wen, C. Wang, and J. Zelek, "Mapping and semantic modeling of underground parking lots using a backpack lidar system," *IEEE Transactions on Intelligent Transportation Systems*, vol. 22, no. 2, pp. 734–746, 2021.

[225] R. Kümmerle, G. Grisetti, H. Strasdat, K. Konolige, and W. Burgard, "g2o: A general framework for graph optimization," in *2011 IEEE International Conference on Robotics and Automation*. IEEE, 2011, pp. 3607–3613.

[226] Z. Liu, C. Suo, S. Zhou, F. Xu, H. Wei, W. Chen, H. Wang, X. Liang, and Y.-H. Liu, "Seqlpd: Sequence matching enhanced loop-closure detection based on large-scale point cloud description for self-driving vehicles," in *2019 IEEE/RSJ International Conference on Intelligent Robots and Systems (IROS)*. IEEE, 2019, pp. 1218–1223.

[227] M. J. Milford and G. F. Wyeth, "Seqslam: Visual route-based navigation for sunny summer days and stormy winter nights," in *2012 IEEE international conference on robotics and automation*. IEEE, 2012, pp. 1643–1649.

[228] W. Chen, H. Zhao, Q. Shen, C. Xiong, S. Zhou, and Y.-H. Liu, "Inertial aided 3d lidar slam with hybrid geometric primitives in large-scale environments," in *2021 IEEE International Conference on Robotics and Automation (ICRA)*. IEEE, 2021, pp. 11566–11572.

[229] P. Yin, L. Xu, J. Zhang, and H. Choset, "Fusionvlad: A multi-view deep fusion networks for viewpoint-free 3d place recognition," *IEEE Robotics and Automation Letters*, vol. 6, no. 2, pp. 2304–2310, 2021.

[230] P. Shi, Q. Ye, Z. Shaoming, and D. Haifeng, "Localization initialization for multi-beam lidar considering indoor scene feature," *Acta Geodaetica et Cartographica Sinica*, vol. 50, pp. 1594–1604, 2021.

[231] P. Shi, J. Li, and Y. Zhang, "Lidar localization at 100 fps: A map-aided and template descriptor-based global method," *International Journal of Applied Earth Observation and Geoinformation*, vol. 120, p. 10336, 2023.

[232] M. Aldibaja, N. Suganuma, R. Yanase, L. Cao, K. Yoneda, and A. Kuramoto, "Loop-closure and map-combiner detection strategy based on lidar reflectance and elevation maps," in *2020 IEEE 23rd International Conference on Intelligent Transportation Systems (ITSC)*. IEEE, 2020, pp. 1–7.

[233] I. A. Barsan, S. Wang, A. Pokrovsky, and R. Urtasun, "Learning to localize using a lidar intensity map," in *Conference on Robot Learning*. PMLR, 2018, pp. 605–616.

[234] Z. Liu, H. Chen, H. Di, Y. Tao, J. Gong, G. Xiong, and J. Qi, "Real-time 6d lidar slam in large scale natural terrains for ugv," in *2018 IEEE Intelligent Vehicles Symposium (IV)*. IEEE, 2018, pp. 662–667.

[235] H. Yin, L. Tang, X. Ding, Y. Wang, and R. Xiong, "Locnet: Global localization in 3d point clouds for mobile vehicles," in *2018 IEEE Intelligent Vehicles Symposium (IV)*. IEEE, 2018, pp. 728–733.

[236] L. Sun, D. Adolfsson, M. Magnusson, H. Andreasson, I. Posner, and T. Duckett, "Localising faster: Efficient and precise lidar-based robot localisation in large-scale environments," in *2020 IEEE International Conference on Robotics and Automation (ICRA)*. IEEE, 2020, pp. 4386–4392.

[237] Y. Jin, Q. Chen, J. Qian, J. Liu, and J. Zhang, "Global localization for single 3d point cloud using voting mechanism," in *2021 6th IEEE International Conference on Advanced Robotics and Mechatronics (ICARM)*. IEEE, 2021, pp. 771–776.

[238] X. Bai, Z. Luo, L. Zhou, H. Fu, L. Quan, and C.-L. Tai, "D3feat: Joint learning of dense detection and description of 3d local features," in *Proceedings of the IEEE/CVF conference on computer vision and pattern recognition*, 2020, pp. 6359–6367.

[239] B. Zhou, Y. He, W. Huang, X. Yu, F. Fang, and X. Li, "Place recognition and navigation of outdoor mobile robots based on random forest learning with a 3d lidar," *Journal of Intelligent & Robotic Systems*, vol. 104, no. 4, pp. 1–26, 2022.

[240] J. Behley and C. Stachniss, "Efficient surfel-based slam using 3d laser range data in urban environments," in *Robotics: Science and Systems*, vol. 2018, 2018, p. 59.

[241] P. Yin, L. Xu, Z. Liu, L. Li, H. Salman, Y. He, W. Xu, H. Wang, and H. Choset, "Stabilize an unsupervised feature learning for lidar-based place recognition," in *2018 IEEE/RSJ International Conference on Intelligent Robots and Systems (IROS)*. IEEE, 2018, pp. 1162–1167.

[242] K. He, X. Zhang, S. Ren, and J. Sun, "Deep residual learning for image recognition," in *Proceedings of the IEEE conference on computer vision and pattern recognition*, 2016, pp. 770–778.

[243] J. Knights, P. Moghadam, M. Ramezani, S. Sridharan, and C. Fookes, "Incloud: Incremental learning for point cloud place recognition," in *2022 IEEE/RSJ International Conference on Intelligent Robots and Systems (IROS)*. IEEE, 2022, pp. 8559–8566.

[244] G. Pandey, J. R. McBride, and R. M. Eustice, "Ford campus vision and lidar data set," *The International Journal of Robotics Research*, vol. 30, no. 13, pp. 1543–1552, 2011.

[245] A. Geiger, P. Lenz, and R. Urtasun, "Are we ready for autonomous driving? the kitti vision benchmark suite," in *2012 IEEE Conference on Computer Vision and Pattern Recognition*, 2012, pp. 3354–3361.

[246] N. Carlevaris-Bianco, A. K. Ushani, and R. M. Eustice, "University of michigan north campus long-term vision and lidar dataset," *The International Journal of Robotics Research*, vol. 35, no. 9, pp. 1023–1035, 2016.

[247] W. Maddern, G. Pascoe, C. Linegar, and P. Newman, "1 year, 1000 km: The oxford robotcar dataset," *The International Journal of Robotics Research*, vol. 36, no. 1, pp. 3–15, 2017.

[248] J. Jeong, Y. Cho, Y.-S. Shin, H. Roh, and A. Kim, "Complex urban lidar data set," in *2018 IEEE International Conference on Robotics and Automation (ICRA)*, 2018, pp. 6344–6351.

[249] J. Behley, M. Garbade, A. Milioto, J. Quenzel, S. Behnke, C. Stachniss, and J. Gall, "Semantickitti: A dataset for semantic scene understanding of lidar sequences," in *Proceedings of the IEEE/CVF International Conference on Computer Vision*, 2019, pp. 9297–9307.

[250] G. Kim, Y. S. Park, Y. Cho, J. Jeong, and A. Kim, "Mulran: Multimodal range dataset for urban place recognition," in *2020 IEEE International Conference on Robotics and Automation (ICRA)*, 2020, pp. 6246–6253.

[251] W. Zhou, J. S. Berrio, C. De Alvis, M. Shan, S. Worrall, J. Ward, and E. Nebot, "Developing and testing robust autonomy: The university of sydney campus data set," *IEEE Intelligent Transportation Systems Magazine*, vol. 12, no. 4, pp. 23–40, 2020.

[252] D. Barnes, M. Gadd, P. Murcett, P. Newman, and I. Posner, "The oxford radar robotcar dataset: A radar extension to the oxford robotcar dataset," in *2020 IEEE International Conference on Robotics and Automation (ICRA)*. IEEE, 2020, pp. 6433–6438.

[253] Y. Liao, J. Xie, and A. Geiger, "Kitti-360: A novel dataset and benchmarks for urban scene understanding in 2d and 3d," *IEEE Transactions on Pattern Analysis and Machine Intelligence*, 2022.

[254] B. Ferrarini, M. Waheed, S. Waheed, S. Ehsan, M. J. Milford, and K. D. McDonald-Maier, "Exploring performance bounds of visual place recognition using extended precision," *IEEE Robotics and Automation Letters*, vol. 5, no. 2, pp. 1688–1695, 2020.